

# Biomechanical Models for Radial Distance Determination by the Rat Vibrissal System

J. Alexander Birdwell,<sup>1</sup> Joseph H. Solomon,<sup>1</sup> Montakan Thajchayapong,<sup>1</sup> Michael A. Taylor,<sup>1</sup> Matthew Cheely,<sup>3</sup> R. Blythe Towal,<sup>2</sup> Jorg Conradt,<sup>4</sup> and Mitra J. Z. Hartmann<sup>1,2</sup>

<sup>1</sup>Departments of Mechanical Engineering and <sup>2</sup>Biomedical Engineering, Northwestern University, Evanston, Illinois; <sup>3</sup>Program in Neuroscience and Cognitive Science, University of Maryland, College Park, Maryland; and <sup>4</sup>Institute of Neuroinformatics, University and ETH Zurich, Zurich, Switzerland

Submitted 7 July 2006; accepted in final form 11 May 2007

**Birdwell JA, Solomon JH, Thajchayapong M, Taylor MA, Cheely M, Towal RB, Conradt J, Hartmann MJZ.** Biomechanical models for radial distance determination by the rat vibrissal system. *J Neurophysiol* 98: 2439–2455, 2007. First published June 6, 2007; doi:10.1152/jn.00707.2006. Rats use active, rhythmic movements of their whiskers to acquire tactile information about three-dimensional object features. There are no receptors along the length of the whisker; therefore all tactile information must be mechanically transduced back to receptors at the whisker base. This raises the question: how might the rat determine the radial contact position of an object along the whisker? We developed two complementary biomechanical models that show that the rat could determine radial object distance by monitoring the rate of change of moment (or equivalently, the rate of change of curvature) at the whisker base. The first model is used to explore the effects of taper and inherent whisker curvature on whisker deformation and used to predict the shapes of real rat whiskers during deflections at different radial distances. Predicted shapes closely matched experimental measurements. The second model describes the relationship between radial object distance and the rate of change of moment at the base of a tapered, inherently curved whisker. Together, these models can account for recent recordings showing that some trigeminal ganglion (Vg) neurons encode closer radial distances with increased firing rates. The models also suggest that four and only four physical variables at the whisker base—angular position, angular velocity, moment, and rate of change of moment—are needed to describe the dynamic state of a whisker. We interpret these results in the context of our evolving hypothesis that neural responses in Vg can be represented using a state-encoding scheme that includes combinations of these four variables.

## INTRODUCTION

Rats use their mystacial vibrissae during navigation and exploratory behaviors to extract three-dimensional (3D) object features, including size, shape, orientation, location, and texture (Andermann et al. 2004; Brecht et al. 1997; Carvell and Simons 1990, 1995; Guic-Robles et al. 1989; Polley et al. 2005; Vincent 1912). To extract these complex 3D features, the rat must at least implicitly estimate the distance from the base of the whisker to the point of object contact. However, the mechanism for radial distance encoding by a single whisker seems problematic, because mechanoreceptors are located only at the base of the whisker, within the follicle (Ebara et al. 2002; Mosconi et al. 1992; Rice et al. 1997). This means that object

position cannot be directly measured by the location of contact on the whisker. Instead, the whisker's interaction with the environment must be transduced into parameters that can be measured at the whisker base.

It is well known that the length of the rat's whiskers varies from long to short along the caudal-rostral dimension (Brecht et al. 1997; Hartmann et al. 2003; Neimark et al. 2003). Thus one plausible mechanism for radial distance encoding is for the rat to compare the identity of whiskers that contacted an object with those that did not. If a whisker of length  $L$  touched an object, but a whisker of length  $L - \Delta L$  did not, the rat could infer that the object was located at a distance between those two values (after accounting for different whisker base locations). Behavioral studies have shown, however, that rats can determine aperture width with only one whisker remaining on each side of the face (Krupa et al. 2001). This suggests that cross-whisker comparisons cannot fully explain the rat's distance discrimination capabilities.

A preliminary analysis of the whisker as a cantilever beam suggested that the stiffness properties of the whisker might provide a mechanical explanation for the rat's ability to perform accurate radial distance discriminations. We specifically hypothesized that information about moment at the whisker base is critical for determining radial object distance. To test this hypothesis, we developed two closely related biomechanical models of the whisker. Both models were deliberately developed in analytic form, so that researchers could easily calculate moment at the whisker base during experiments. The analytical models were tested against numerical simulations to quantify limits on their application and together confirmed our hypothesis: by correlating movement to changes in moment at the whisker base the rat could determine the radial distance of an object.

This work continues our characterization of vibrissa dynamics (Hartmann et al. 2003) and suggests some useful ways to represent the mechanical information encoded in the primary sensory neurons of the trigeminal ganglion (Vg). We interpret these results in the context of our evolving hypothesis that neural responses in Vg can be comprehensively represented using a state-encoding scheme that includes combinations of four and only four mechanical variables at the whisker base:

Address for reprint requests and other correspondence: M.J.Z. Hartmann, Depts. of Mechanical and Biomedical Engineering, Northwestern Univ., 2145 Sheridan Rd., Evanston, IL 60208-3111 (E-mail: m-hartmann@northwestern.edu).

The costs of publication of this article were defrayed in part by the payment of page charges. The article must therefore be hereby marked "advertisement" in accordance with 18 U.S.C. Section 1734 solely to indicate this fact.

angular position, angular velocity, moment, and rate of change of moment.

## METHODS

### *Whisker preparation for static and dynamic experiments*

This analysis is based on a total of seven vibrissae obtained from three female Sprague-Dawley rats that had been euthanized in unrelated experiments. All procedures were approved in advance by Northwestern University's Animal Care and Use Committee. Each whisker was grasped firmly at the base and plucked out of the follicle for testing. Visual examination of the whisker revealed that there was a qualitative difference in appearance between approximately the first millimeter of the whisker and the remainder of the whisker. Closer examination under the microscope additionally suggested that this first millimeter is approximately the portion of the whisker that would reside in the follicle, and we therefore used this portion to rigidly attach the whisker to the test stand or load cell during experiments.

### *Static experiments to determine whisker flexural characteristics*

A micromechanical force tester (Mach-1, BioSyntech, Montreal, Canada), was used to impose small vertical displacements on the whisker at known horizontal distances from the base and to measure the associated force. The Mach 1 has a positional accuracy of  $1.5\ \mu\text{m}$ , and we used a 50-g load cell to achieve a load resolution of  $0.0025\ \text{g}$ . This allowed us to characterize force-bending relationships for all but the smallest whiskers. Images of the whiskers as they were deflected during the experiment were acquired with a high-resolution ( $3,088 \times 2,056$  pixels) digital camera (Digital EOS Rebel, Canon).

Figure 1A shows the experimental set up used to perform the static force measurements. Whiskers were rigidly fixed at their base to a cylindrical metal test stand using cyanoacrylate (superglue). All whiskers were mounted concave down. A shallow groove  $1\ \text{mm}$  in length was etched in the top face of the stand. The whisker was placed directly in the groove to ensure that exactly the first millimeter of the whisker was rigidly attached to the stand. As described above, this first millimeter is likely to correspond to the portion of the whisker that would normally reside inside the follicle. Miniature scales (Mini-tool, Los Gatos, CA) with  $100\text{-}\mu\text{m}$  tick-marks were attached both vertically and horizontally to the side of the cylindrical stand. These

scales provided an independent measure of displacement that could be compared with the positions given by the Mach-1 micromechanical tester. The inset of Fig. 1A shows a close-up view of the stimulator used to deflect the whisker. The stimulator was custom-machined to a fine taper so that the width that ultimately contacted the whisker was  $\sim 500\ \mu\text{m}$ .

At the beginning of each static experiment, the stimulator was rigidly attached to the Mach-1 load cell and carefully positioned in both  $x$ - and  $y$ -directions. In the  $x$ -direction, the stimulator was positioned at the rightmost edge of the test stand, and this position was defined as  $x = 0$ . In the  $y$ -direction, the stimulator was positioned just above the surface of the whisker as close as possible while measuring zero load. This position was defined as  $y = 0$ . The stimulator was lowered in small ( $100\ \mu\text{m}$ ) intervals in the  $y$ -direction (computer-controlled using the Mach-1 micromechanical tester) to precisely displace the stationary whisker. The stimulator was lowered until the whisker had been deflected  $1,500\ \mu\text{m}$  ( $1.5\ \text{mm}$ ). Forces from the load cell were recorded at every step for every whisker, and digital pictures of the whisker's bending were taken at every step for all seven whiskers. Note that in these static experiments, the load cell measured the vertical force necessary to displace the whisker a known vertical distance, at a particular distance from the whisker base. It did not measure the force at the base of the whisker.

After the whisker had been deflected through a full  $1,500\ \mu\text{m}$ , the stimulator was moved back to  $y = 0$  so that it no longer contacted the whisker. The stimulator was moved in the positive  $x$ -direction to a different horizontal distance from the base of the whisker. We typically moved the stimulator in  $2,000\text{-}\mu\text{m}$  increments in the  $x$ -direction, but for some whiskers we moved in  $1,000\text{-}\mu\text{m}$  intervals. The stimulator was again positioned carefully just barely above the surface of the whisker, this position was defined as a new  $y = 0$ , and the stimulator was lowered to displace the whisker at this new  $x$ -location. We continued moving the stimulator further out horizontally from the base of the whisker until we reached the resolution of the force measurement capabilities of the Mach 1 tester.

### *Dynamic experiments to determine whisker flexural characteristics*

In dynamic experiments, the whisker base was mounted directly to the load cell and moved using the Mach-1 tester to hit the tapered stimulator, which was held fixed in position. This experimental setup

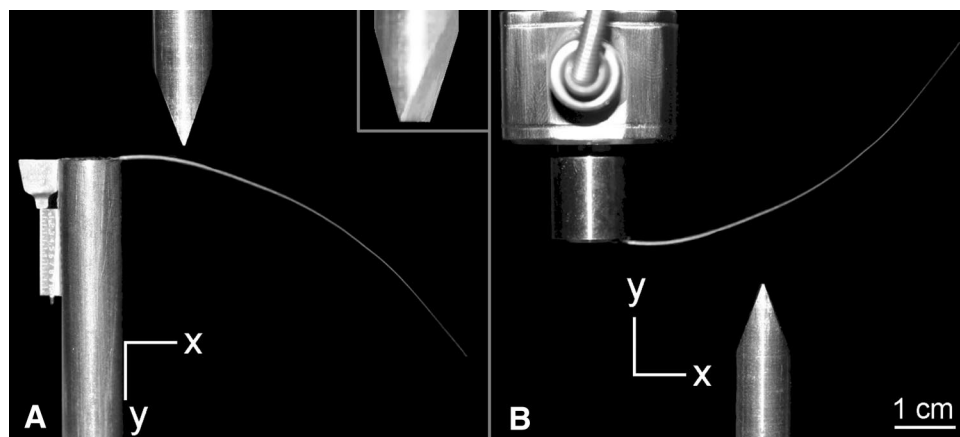


FIG. 1. Experimental measurement of static and dynamic forces. *A*: in static experiments, the first  $1\ \text{mm}$  of each plucked whisker was glued rigidly to a cylindrical post with horizontal and vertical scales fixed to the left side. A tapered stimulator (*inset*: side view) attached to a load cell was gradually lowered into the whisker at different distances from the whisker base. Load cell thus directly measured force necessary to displace the whisker a known vertical distance ( $y$ ), at a particular radial distance ( $x$ ). *B*: in dynamic experiments, the base of the whisker was mounted directly to the load cell and translated into the tapered stimulator. Note that the  $y$ -axis is reversed for directional consistency. Tapered stimulator was held fixed and positioned at different radial distances from the whisker base. Under these conditions, the load cell directly measured force at the whisker base as the whisker was increasingly deflected over time, at a particular radial distance. In both static and dynamic experiments, the contact width of the stimulator on the whisker was  $\sim 500\ \mu\text{m}$ .

is shown in Fig. 1B and allowed us to continuously monitor the force at the base of the whisker as it deflected into the stimulator. We lowered each whisker into the stimulator at two different velocities (50 and 500  $\mu\text{m/s}$ ) and at five different horizontal locations away from the whisker base (3, 5, 7, 9, and 11 mm). Note that the  $y$ -direction is opposite that in Fig. 1A for directional consistency with respect to the whisker.

### Analysis of experimental data

Force and displacement data (from the Mach-1 tester), along with the digital images of the whiskers, were imported into MATLAB (v 7.0 2004, The Mathworks, Natick, MA). As is the convention for load cells, the load measurements from the Mach-1 were provided in grams. These measurements were multiplied by a factor of 9.8  $\text{m/s}^2$  to obtain the force in millinewtons (mN). Whisker-stimulator contact forces were always assumed to be normal to the whisker because the contribution of force from friction was assumed to be negligible. The load cell in the Mach-1 tester measured only vertical force, and we therefore divided the measured force by the cosine of the whisker angle at the contact point to obtain the actual force applied.

To extract the geometrical shapes of the whiskers from the high-resolution photographs, the upper and lower outlines of the whisker were located using semiautomated image processing techniques in MATLAB. The shape of the whisker was defined as the average of the upper and lower outlines. For each extraction the averaged points were overlaid on top of the photographed whisker to visually confirm that the averaging technique yielded data points that fell within the upper and lower outlines of the whisker, thus giving an excellent match to the overall shape.

### Fundamentals of elasticity: cantilever beam theory

Our goal in this research was to develop an accurate but simple biomechanical model of the rat whisker as a cantilevered beam. Cantilever beam models are derived from elasticity theory (Euler 1744; Love 1944; Timoshenko 1970; Young and Budynas 2001), which can be used to relate the curvature,  $\kappa$ , of a straight cantilever beam to the moment,  $M$ , at each point along its length,  $x$

$$\kappa(x) = \frac{\frac{d^2y}{dx^2}}{\left[1 + \left(\frac{dy}{dx}\right)^2\right]^{\frac{3}{2}}} = \frac{M(x)}{EI} \quad (1)$$

In Eq. 1,  $y(x)$  is the displacement of the beam at each  $x$  location along the length,  $E$  is Young's modulus (also called the elastic modulus), and  $I$  is the area moment of inertia. In general, Eq. 1 can only be solved numerically, but for small angle deflections (less than  $\sim 14^\circ$ ), the term  $\left(\frac{dy}{dx}\right)^2$  in the denominator is negligible and Eq. 1 can be linearized as

$$\kappa(x) = \frac{d^2y}{dx^2} = \frac{M(x)}{EI}, \quad (2)$$

where

$$M(x) = \begin{cases} F(a-x), & 0 \leq x \leq a \\ 0, & a \leq x \leq L \end{cases}$$

In Eq. 2,  $F$  is the force exerted normal to the beam at a distance along the whisker,  $a$ , from the base of the beam. The linearization assumes that the beam is initially straight and that it deflects only through small angles. This means that the arc length distance  $a$ , is essentially the same as a horizontal distance.

If we now assume that the beam is cylindrical with a radius of  $r$  then the area moment of inertia  $I = \pi r^4/4$  and Eq. 2 can be solved analytically for  $y(x)$

$$y(x) = \begin{cases} \frac{F}{6EI} (3x^2a - x^3), & x \leq a \\ \frac{F}{6EI} (3a^2x - a^3), & x \geq a \end{cases} \quad (3)$$

Note that  $y(x)$  is linear with horizontal position  $x$  for values of  $x$  greater than  $a$ . We adapted this model of the cylindrical beam into a model for the tapered beam (see RESULTS and APPENDIX A) to more accurately represent the morphology of real rat whiskers.

It is important to note that elasticity theory itself is very general, simply relating curvature to moment. However, for biological materials, Young's modulus ( $E$ ) is an approximation at best, because these materials are typically anisotropic, heterogeneous, and nonuniform. For a material whose value of  $E$  is roughly 5 GPa, the best one might expect is to obtain a value correct to within a few gigapascals.

### Comparing results of model 1 with experimental results

Our analysis required a comparison of the shape of the whisker as predicted by our tapered beam model (RESULTS, model 1) with the shape of the real whisker obtained experimentally with high resolution photography. However, real rat whiskers have an inherent curvature. We therefore made the approximation that the deflection of the real whisker (under a force  $F$  at a particular arc length location,  $a$ ) could be expressed as the deflection of a straight tapered cantilever beam (under that same force  $F$ , imposed at the same location  $a$ ), summed with the inherent curved shape of the undeflected whisker (under conditions of zero force). This approximation is schematized in Fig. 2. This analysis is valid as long as the assumptions of the linearized beam model are not violated, namely that the deflections and inherent whisker curvature are sufficiently small. The first part of RESULTS identifies the conditions in which these assumptions are valid.

Summing the deflection of the tapered cantilever beam (from analytical equations) with the inherent curvature of the undeflected whisker (from photography) required some careful geometrical analysis. The summation process involved three steps and is schematized in Fig. 2. First, thousands of nodes along the (real, undeflected) whisker were placed at constant arc length (Fig. 2A). Second, the arc lengths from the base of the whisker to each of the nodes were used as the  $x$ -values in the deflection equation to analytically solve for the small-angle deflection of a tapered cantilever beam (RESULTS, Eq. 5). Figure 2B shows the magnitude of the vertical deflection for each node. For small angles, the path of deflection can be assumed to follow a vertical translation instead of an arc (Young and Budynas 2001). Third, the resulting deflection values were added to each node along the undeflected whisker in an inward-pointing normal direction to the whisker at each node (Fig. 2C). This three-step procedure has a very intuitive underpinning: it simply ensured that equivalent deflections were summed between the theoretical model and the experimentally obtained photographs.

Note that for this model, nodes beyond the point of whisker-stimulator contact deflect linearly, as can be seen mathematically in Eq. 3. In the model, we could therefore assume that the portion of the whisker past the stimulator contact point was translated in the same direction as the last node before the stimulator contact. This portion of the whisker was thus aligned to match the tangent of the deflected whisker at the point of contact.

### Numerical simulations

Numerical simulations of whisker bending were performed to identify the limitations on and validate the results of the two analytical models. These numerical simulations also accounted for large angle

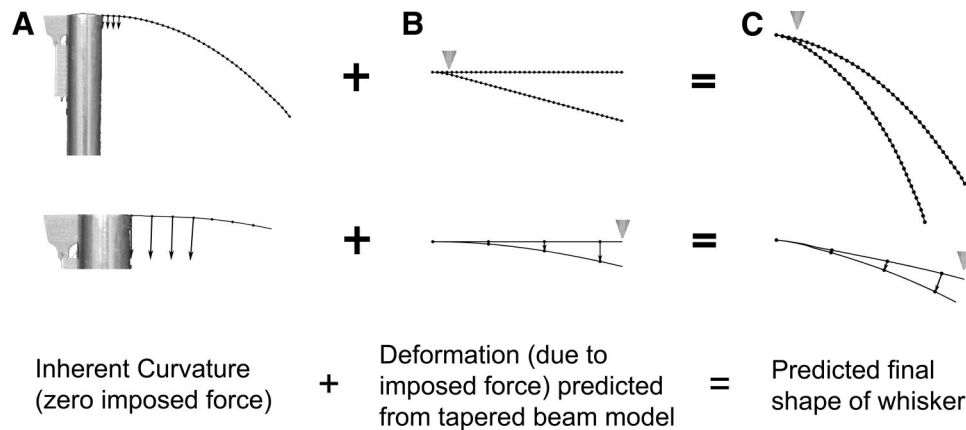


FIG. 2. Geometrical method used to predict the final shape that a whisker will assume under an imposed force. Predicted whisker shape was found by summing the inherent curvature of the whisker (from a photo) with the curvature resulting from an imposed force as predicted by the tapered beam model. *Top row:* deflections of entire whisker. *Bottom row:* enlarged versions of region near the base for visual clarity. In each figure, upside-down triangle indicates position of applied force. *A, top:* under conditions of zero force, the (undeflected) shape of the whisker was extracted from a photograph and partitioned with nodes spaced at equal arc-lengths. This quantified the inherent curvature of the whisker. *Bottom:* inward pointing unit normal was found for all nodes between the base of the whisker and the stimulator contact point. *B, top:* *model 1* was used to predict deflection of a linearly tapered cantilever beam with the same dimensions as the real whisker (base diameter and length). Modeled beam was partitioned with equally spaced nodes as in *A*. *Bottom:* vertical distance that each node traveled from undeflected to deflected case was found. *C, top and bottom:* magnitude of vertical deflection for each node in *B* was added to its corresponding node in *A*, in the associated unit normal direction shown in *A (bottom)*. It is clear from *C (top)* that even a very small deflection imposed near the whisker base can have a large effect on the position of the tip of the whisker.

deflections and inherent whisker curvature. All simulations were performed in MATLAB, and were based on the following principle: if a force  $\vec{F}$  acts at an arc-length  $a$  from the base of a beam, the resulting beam shape can be found through repeated application of  $d\kappa_i = (\vec{r}_i \times \vec{F})/EI_i$ , where  $d\kappa_i$  is the change in curvature,  $\vec{r}_i$  is the vector connecting node  $i$  to  $a$ , and  $I_i$  is the area moment of inertia at node  $i$ .  $F$  always acts normal to the whisker as long as there is no friction.

## RESULTS

We began by considering how best to realistically model a rat whisker. We noted three inadequacies of the analytical model of the cylindrical cantilever beam presented in *Eqs. 2* and *3*: 1) the model assumes a cylinder, but the real whisker is tapered, as a cone; 2) the model assumes a straight beam, but the real whisker has inherent curvature; and 3) the model is linearized, assuming only small angle deflections (no more than  $\sim 14^\circ$ ), but the real whisker can bend through very large angles during object contact.

The results below account for each of these three complexities and are divided into three parts. In part 1, we develop an analytical model (*model 1*) to describe the bending of a rat whisker. The model uses the magnitude and location of the imposed force to determine the resultant shape of the whisker after deflection. The model accounts for both whisker taper and inherent whisker curvature and limits on its applicability are tested using numerical simulations.

In part 2, we validate *model 1* against experimental data obtained from real rat whiskers, showing an excellent match between theory and experiment. Finally, in part 3, we develop a second analytical model (*model 2*) that describes the relationship between the rate of change of moment at the whisker base and radial object distance. Numerical simulations are used to show that the inherent curvature of the whisker has a negligible effect on this relationship. We show that measuring changes in moment at the whisker base would permit the rat to extract radial object distance and analyze the consequences of this result for coding in the trigeminal ganglion.

### Part 1: Developing an analytical model of a tapered rat whisker with inherent curvature

AN ANALYTICAL EXPRESSION FOR THE DEFORMATION OF A TAPERED WHISKER WITH NO INHERENT CURVATURE. Expressions for the deflection of a straight cylindrical cantilever beam under a load are readily available in the literature (Young and Budynas 2001). However, the diameter of a rat whisker decreases approximately linearly with length (Hartmann et al. 2003; Neimark et al. 2003). We therefore extended the cylindrical model to account for the taper of the whiskers. The basic derivation for tapered deflections is the same as for the cylindrical case and can be found in APPENDIX A. The analytic solution for the small-angle deflections of a tapered beam was found to be

$$y(x) = \begin{cases} \frac{2FLx^2}{3E\pi r_{\text{base}}^4} \left( \frac{3La - Lx - 2ax}{(L-x)^2} \right), & x \leq a \\ \frac{2FLa^2}{3E\pi r_{\text{base}}^4} \left( \frac{3Lx - La - 2ax}{(L-a)^2} \right), & x \geq a \end{cases} \quad (4)$$

Comparison of *Eq. 4* with *Eq. 3* shows clearly that a whisker's taper has a substantial effect on its deformation characteristics; these effects are quantified in detail in APPENDIX B.

EFFECTS OF TAPER ON THE SMALL ANGLE APPROXIMATION. The small angle assumption implicit in the linearization of *Eq. 1* means that the deformations expressed in *Eq. 4* will become inaccurate after a certain bending angle. We used numerical simulations (see METHODS) to explore how linearization impacts the accuracy of the analytical model under large angle deflections and inherent whisker curvature.

Figure 3A shows the difference between the small-angle approximation and the large-angle numerical result for a 200- $\mu\text{N}$  force applied at distances of 10, 20, and 30 mm out along a 60-mm tapered whisker. For the first two locations of applied force, the difference between the small angle approximation (dotted line) and the numerical result (solid line) is

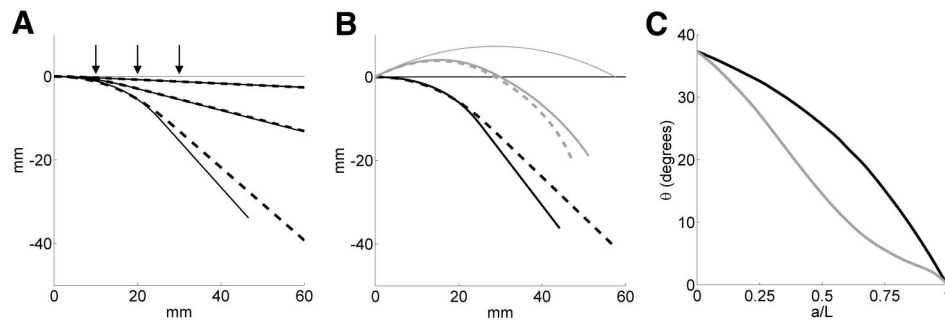


FIG. 3. Effects of taper and inherent curvature on the small angle approximation. *A*: effect of small-angle approximation is exemplified by imposing a 200- $\mu\text{N}$  force at 10, 20, and 30 mm from the base of a straight, tapered 60-mm whisker and comparing the small-angle (linearized, analytic) and large-angle (numerical) results. Results using the small angle approximation are shown as dotted lines, and results for the full numerical solution are shown as solid lines. Because deflections increase as force is exerted further from the base, the small angle assumption begins to break down and curves accordingly diverge. *B*: comparison of analytical and numerical results after including effects of inherent whisker curvature. Thin lines represent an undeflected straight whisker (black, overlaps with the x-axis) and an undeflected curved whisker (gray). Normalized curvature of the curved whisker is 1. In simulation, an increasingly large force was applied at  $a = 30$  mm until magnitude of predicted deflection  $y(a)$  differed by 10% between analytic and numerical results. Thicker black (initially straight) and gray (initially curved) lines represent results of analytic (dashed) and numerical (solid) solutions. Analytical model does an excellent job of predicting shape of the whisker up to  $a$ , but is less accurate beyond the point of contact. *C*: accuracy of analytical model depends on location of imposed force. An increasingly large force was applied at several points along a tapered, straight whisker (black) and a tapered, curved whisker with unity normalized curvature (gray) until the predicted deflection  $y(a)$  disagreed by 10% between analytic and numerical results. Values on the y-axis represent the angle  $\theta$  that is achieved when the 10% threshold is reached. Analytical model clearly performs best when force is applied close to the base. It is also apparent that taper has a moderate effect on the accuracy of the analytic model.

negligible. When the force is applied at 30 mm, the small angle approximation clearly diverges from the numerical result as the deflection angle becomes sufficiently large. The effect of taper increases for deflections applied further from the base.

**MODEL 1: DEFORMATION OF A TAPERED WHISKER WITH INHERENT CURVATURE.** The simplest way to incorporate curvature into the analytical expression for a straight, tapered whisker (Eq. 4) is to sum the inherently curved shape of the real undeflected whisker with the deflection of a straight, tapered cantilever beam. Our first model performed this summation according to the method depicted in Fig. 2.

To validate the assumptions implicit in the summation, we used numerical simulations to calculate the deflections of an inherently curved whisker through large angles (see METHODS). Before we could compare the analytical results of *model 1* and the results of the numerical simulations, however, we noted one additional complexity, as follows: if the whisker is initially straight and deforms only through small angles, the arc length  $a$  (the distance as measured along the length of the whisker) differs negligibly from the straight distance from whisker base to point  $a$  out along the whisker. This was discussed previously in METHODS. If the whisker is not straight, but instead has an inherent curvature, these two values are different. Thus for the remainder of this paper, it is important to remember that  $a$  is always defined as the arc length distance, not the straight distance from base to point of contact distance.

Figure 3*B* shows the error between deflection profiles found using *model 1* and using numerical simulations. The thin solid lines represent straight (black) and inherently curved (gray) whiskers. The inherently curved whisker was chosen to have a constant normalized curvature (ratio between the total arc length and the radius of curvature) of 1. This normalized curvature value is similar to the values found for the whiskers used in this study (data not shown). An increasingly large force was applied at  $a = 30$  mm for both whiskers until the magnitude of deflection at  $a$ ,  $y(a)$ , differed by 10% between the two models. The thick solid and dashed lines give the deflected shape of the initially straight (black) and curved (gray) whis-

kers, as found by using *model 1* (dashed) and numerical simulation (solid). It is clear that *model 1* yields an accurate description of the deflected whisker up to the force location  $a$ , but is less accurate further out.

Figure 3*C* quantifies the amount of angular deflection that results in 10% error between the two models for a force imposed at any point along the whisker. The inherently curved whisker again had normalized initial curvature of 1, as described for Fig. 3*B*. The same procedure described for Fig. 3*B* was repeated for several  $a$  values and the resultant deflection angle,  $\theta$ , at which 10% error was reached for each  $a$  value was recorded. Figure 3*C* shows the amount of angular deflection plotted against normalized location of the imposed force,  $a/L$ , for an inherently straight (black) and curved (gray) whisker. It is apparent from this figure that imposed force location affects the amount of deflection possible before 10% error results between *model 1* and the numerical simulations. As the location of imposed force increases, the amount of deflection before the 10% threshold is reached decreases for both the straight and precurved whiskers. This relationship is steeper for the inherently curved whisker, but both cases show that *model 1* is most accurate when forces are applied close to the whisker base.

This analysis has shown that by summing the inherently curved shape of the real whisker with the deformations calculated from Eq. 4, experimenters can obtain an approximation of the deflected whisker shape up to point  $a$  with  $\leq 10\%$  error, provided the force is imposed at  $a/L < 70\%$ .

#### Part 2: Validating *model 1* against experimental data obtained from real rat vibrissae

*Model 1* incorporates the effects of taper and inherent curvature, and we have shown it to be particularly accurate for forces applied close to the base. We used two different methods to determine how well *model 1* captured the bending characteristics of a real rat whisker. First, we compared force-displacement curves between model and experiment. Second,

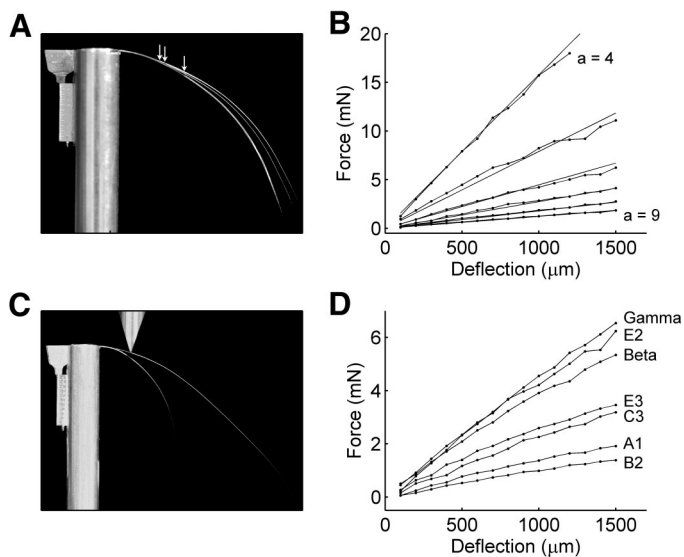


FIG. 4. Matching force-displacement curves between theory and experiment. **A:** superimposed images of the E2 whisker, bending as a force  $F = 121.8 \pm 24.5 \mu\text{N}$  is imposed at 3 different locations (arrows). **B:** relation between deflection and force needed to cause that deflection is approximately linear for any given point where force is imposed. Solid lines represent expected force-deflection relationship derived from *model 1* using a Young's modulus of 2.6 GPa, whereas dotted lines represent experimental data where deflections were imposed at evenly spaced horizontal distances from the base (4–9 mm). **C:** shorter whiskers deflect more than longer whiskers when the same load is applied. Bending of whiskers C3 (short whisker) and Beta (long whisker) is shown here. **D:** whiskers have unique geometrical dimensions, which result in different force-deflection relationships. Each whisker was tested with force imposed 6 mm horizontally from the base.

we used the model to predict the entire shape of deflected whiskers, and compared this prediction with experimentally-obtained shapes of deflected whiskers.

**FORCE DISPLACEMENT CURVES: ANALYTICAL EQUATIONS AND EXPERIMENT.** We experimentally quantified bending for a real rat whisker in response to a force imposed at different distances from the base. Figure 4A shows three overlaid images of the E2 whisker bending under the same force ( $121.8 \pm 24.5 \mu\text{N}$ ) imposed at a distance of 7, 8, and 11 mm horizontally from the base. Note that although during experiments the stimulator was positioned at horizontal distances, during all analysis the horizontal distance was converted to arc-length.

Figure 4A clearly shows that when a force is imposed further away from the base, the whisker deflects more. This effect is quantified in Fig. 4B, in which forces are imposed at different distances (4, 5, 6, 7, 8, and 9 mm horizontally from the base of the E2 whisker). The solid lines are the theoretical force-deflection relationship predicted from Eq. 4. The dotted lines indicate experimental data. In Eq. 4, we used the measured diameter ( $232 \mu\text{m}$ ) to calculate  $I = 1.42 \times 10^{-16} \text{m}^4$ . The measured length of the whisker was 48.0 mm, and a good fit for  $E$  was found to be 2.6 GPa. For these values of  $E$  and  $I$ , an excellent match was found between Eq. 4 and experiment.

Figure 4C shows superimposed images of the C3 and  $\beta$  whiskers as they were deflected by approximately the same force ( $840.3 \pm 94 \mu\text{N}$ ) imposed at a horizontal distance of 8 mm. It is clear that the force has a larger effect on the C3 whisker ( $D_{\text{base}} = 119 \mu\text{m}$ ,  $L = 21.50 \text{mm}$ ) than on the  $\beta$  whisker ( $D_{\text{base}} = 225 \mu\text{m}$ ,  $L = 66.20 \text{mm}$ ). Figure 4D quan-

tifies this effect for seven different whiskers of varying size. In this experiment, whiskers  $\beta$  and  $\gamma$  are the longest whiskers, with lengths of 66.2 and 60.3 mm, respectively, whereas E2 and  $\beta$  are the thickest at the base, with base diameters of 232 and  $225 \mu\text{m}$ , respectively. The last four whiskers are all shorter and thinner at the base than  $\beta$ ,  $\gamma$ , or E2, and therefore require less force to deflect the same amount.

Notably, Fig. 4D shows that at a given horizontal distance away from the base (6 mm in this case) the force-displacement curve follows a linear relationship for each whisker. This relationship can be seen explicitly in Eq. 4. Importantly, this does not mean that for a given force  $F$  the whisker will bend linearly along its length, because the proportionality constant between  $F$  and  $y(x)$  is different at each point  $x$ .

**CAPTURING THE COMPLETE SHAPE OF A WHISKER: MODEL 1 COMPARED WITH EXPERIMENT.** The force-displacement curves in Fig. 4 showed a good match between Eq. 4 and experiment for discrete values of force and displacement. They also serve to quantify the effects of whisker size (base diameter and length) and force location on whisker deflection. However, the curves of Fig. 4 only quantify the relation between force and displacement at point  $a$ , where the force is applied. How well can *model 1* as described in part 1 characterize the entire shape of the whisker when it contacts an object, purely as a function of whisker length, diameter, and object distance  $a$ ? To answer this question, *model 1* was used to predict the deflection of the whisker everywhere along its length (i.e., at all values of  $x$ ). These modeling results were then compared with the photographed shape of the whisker (Fig. 1A). Because Fig. 3C shows that the model should remain accurate for relatively large deflections close to the base, it would be surprising if model and experiment were not in good agreement.

We used *model 1* to calculate the full shape of the whisker as a function of  $x$  analytically while leaving Young's modulus ( $E$ ) as a free parameter. Experimentally, we took digital photographs to obtain the entire shape of each whisker as it was increasingly deflected by the stimulator. We imported the photographed shape into MATLAB and superimposed the modeling result. The value of  $E$  was varied in the model until the best match was found between model and experiment. If  $E$  was too large, the model did not deflect enough compared with the experimentally deflected whisker, and if  $E$  was too small, the model whisker deflected too much.

The *inset* of Fig. 5 shows the quantities used to find the best match between model and experiment. The error between the model and the experimental data were found by taking the ratio of the areas between the model and the deflected whisker (*area 2*) and the area between the deflected whisker and the undeflected whisker (*area 1 + area 2*). All areas were calculated from the whisker base to the point of contact,  $a$ . Normalization to the area between the undeflected whisker and the deflected whisker accounted for any error induced by apparent changes in length due to the small angle approximation, and permitted comparisons of error estimates across whiskers of different lengths. This ratio is referred to as the percent area error, plotted on the  $y$ -axis of Fig. 5.

Seven whiskers (A1, B2,  $\beta$ , C3, E2, E3,  $\gamma$ ) were used in the analysis of the complete whisker shape. For each whisker, we averaged over all vertical deflections at each hori-

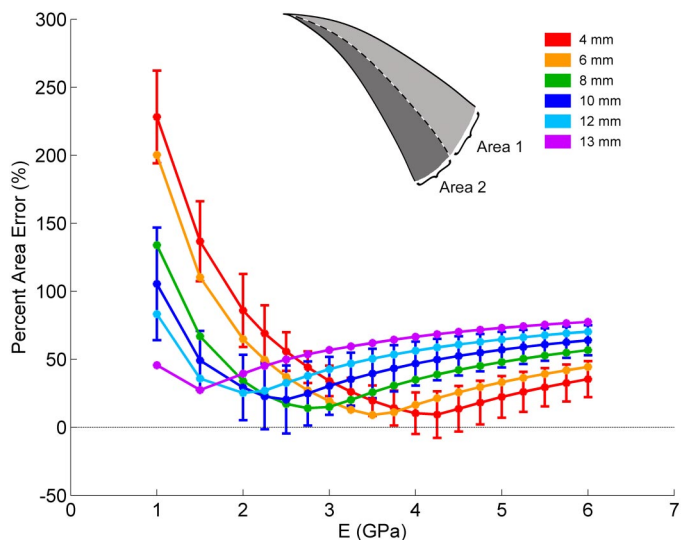


FIG. 5. *Model 1* accurately captures the shape of the entire whisker during deformation. *Inset*: how error between model and experiment was calculated. Top solid line represents undeflected whisker, center dotted line is model of deflected whisker, and bottom solid line is deflected whisker as measured experimentally. *Area 1* represents difference between modeled deflected whisker and undeflected whisker. *Area 2* represents difference between modeled deflected whisker and experimental data. “Percent area error” was defined as the ratio of area 2 to the sum of areas 1 and 2. This measure normalized error over different whisker lengths and stimulator placements. Plot shows percent area error between model and experiment for changing values of Young’s modulus for the A1 whisker. Each trace represents average of percent error over 15 vertical displacements at a single horizontal distance from the whisker base as indicated in legend. Best fits were obtained with values of Young’s modulus that ranged between 1.5 and 4.25 GPa, with an average of  $E = 2.75$  GPa. For visual clarity, standard deviations are shown on only 2 traces (blue and red), displaying largest and smallest error ranges.

zontal distance from the base. This amounted to  $\sim 110$  comparisons between experiment and model,  $>20$  values of Young’s modulus, for a total of  $\sim 2,200$  comparisons per whisker.

Figure 5 shows the results for the A1 whisker. Plotting error as a function of Young’s modulus ( $E$ ) shows that 1) the smallest error (2.72% for the A1 whisker) is found when the object is closest to the base of the whisker, 2) estimated  $E$  for the A1 whisker has a range of  $\sim 1.5\text{--}4.3$  GPa, with an average of 2.75 GPa, consistent with the value found for Fig. 4B and with previous estimates (Hartmann et al. 2003; Neimark et al. 2003), and 3) the value of the “best”  $E$  decreases as the object moves further from the base. These results were representative of all whiskers. A1 does not represent a “best case.”

The ranges for  $E$  of the other whiskers were mostly similar to that of A1. Table 1 shows geometrical dimensions and average values of  $E$  for all seven whiskers. Results for the C3 whisker lay outside the range of results for the other whiskers. For C3, Young’s modulus ranged from 4 to 9.5 GPa and had an average value of 6.25 GPa. The C3 whisker was by far the shortest and thinnest of the whiskers and deflections were imposed up to  $\sim 50\%$  along the whisker length. Most other whiskers only had deflections imposed up to  $\sim 35\%$  along the length of the whisker. This could help explain the large value of Young’s modulus found for the C3 whisker.

*Part 3: A biomechanical model for extracting radial object distance using information about moment*

**MODEL 2: AN ANALYTICAL EXPRESSION FOR RADIAL OBJECT DISTANCE AS A FUNCTION OF MOMENT AT THE WHISKER BASE.** *Equation 4* describes a relationship between the deflection,  $y(x)$ , at each point,  $x$ , along a tapered whisker and the arc length,  $a$ . The value of  $y(x)$  is related to  $a$  through the force  $F$  imposed at point  $a$ , the bending stiffness represented by the product  $EI_{\text{base}}$ , and the total arc length,  $L$ , of the whisker. We asked whether the rat could use the relationship expressed in *Eq. 4* to infer information about the radial object distance  $d$ , from the whisker base to the contact point. Note that in general the distance  $d$  is shorter than arc length distance  $a$ , however, assuming a straight whisker and evaluating *Eq. 4* at  $y(d)$  yields

$$y(d) = \frac{FLd^3}{3EI_{\text{base}}(L - d)} \tag{5}$$

Using  $M = d \times F$  and  $\theta = y(d)/d$  (assuming small angle deflections) yields

$$M = C\theta \left( \frac{1}{d} - \frac{1}{L_{\text{BT}}} \right) \tag{6}$$

where  $C = 3E \frac{\pi r_{\text{base}}^4}{4} \equiv 3EI_{\text{base}}$  and  $L_{\text{BT}}$  is the linear base to tip length of the whisker. Note that  $L$  was replaced with  $L_{\text{BT}}$  to enforce the boundary condition that  $M = 0$  when  $d = L_{\text{BT}}$ . Solving for the variable  $d$ , and taking time derivatives yields

$$d = \frac{C\dot{\theta}L_{\text{BT}}}{C\dot{\theta} + ML_{\text{BT}}} \tag{7}$$

*Equation 7* represents our second analytical model. It relates radial object distance to change in moment at the whisker base.

Note that *Eq. 7* is expressed in terms of time derivatives. These time derivatives are included primarily for biological plausibility. Recall that  $\theta$  represents the angle that the whisker has rotated since the time of initial contact with the object.  $M$  is the moment experienced at the base, which increases as the whisker rotates against the object. In an engineered system, it is easy to set  $\theta = 0$  at the angle of initial contact and to keep track of its increasing value. In principle, just like the engineered system, the rat could use the absolute position of the whisker ( $\theta$ ) combined with an absolute measurement of moment to determine object distance. However, given the well-known difficulty for the nervous system to accurately measure

TABLE 1. *Geometrical whisker dimensions and calculated values for average Young’s modulus (E)*

| Whisker Name | Arc Length, mm | Base Diameter, $\mu\text{m}$ | Average E, GPa |
|--------------|----------------|------------------------------|----------------|
| $\beta$      | 66.2           | 225                          | 1.40           |
| $\gamma$     | 60.3           | 199                          | 3.75           |
| A1           | 51.7           | 160                          | 2.75           |
| E2           | 48.1           | 232                          | 1.90           |
| B2           | 41.1           | 169                          | 2.30           |
| E3           | 33.3           | 189                          | 3.90           |
| C3           | 21.5           | 119                          | 6.25           |

The best fit Young’s modulus was found at each combination of deflection amplitude and contact distance. Average  $E$  was calculated as the mean of all best fits.

absolute quantities, but its exquisite sensitivity to rates of change, we think it most probable that the rat would use the time derivatives as represented in Eq. 7.

If the whisker moves at constant velocity, then derivatives of moment with respect to  $\theta$  and with respect to time are proportional. If, in contrast, the whisker moves at nonconstant velocity, the rat could keep track of how moment is changing relative to  $\theta$ . Thus most generally, radial distance can be computed as

$$d = \frac{CL_{BT}}{C + (dM/d\theta)L_{BT}} \quad (8)$$

The fact that the computation can be performed at every instant in time—and for varying whisking velocities—is a key advantage of the proposed mechanism for determining object distance. It seems likely that a particularly good time for the rat to measure moment and angle would be immediately following contact up until the point in time when the linearization breaks down. For example, a constant protraction velocity of  $400^\circ/\text{s}$  would allow  $\sim 2^\circ$  of rotation in the 5 ms after object contact, well within the linear range. It should be noted that the rat will have much less time to compute object distance if contact occurs close to the tip, as the whisker will quickly fold in on itself and/or flick past the object for small  $\theta$ , and  $\dot{M}$  will change accordingly.

Equations 7 and 8 show that, if the rat can keep track of the rate of change of moment and the velocity with which it is “pushing” its whisker against the object, enough information will be present to infer object distance. Taken with the results of previous studies that have described mechanisms for encoding horizontal and vertical position (Ahissar and Arieli 2001; Ahissar et al. 2000; Szwed et al. 2006), these equations effectively show that only three mechanical variables are required to extract 3D spatial information about objects. Those variables are angular position, angular velocity, and rate of change of moment (or curvature). In addition to these three variables, we posit that the rat is sensitive to a fourth variable—moment—so as to remain sensitive to static deflections of its whiskers.

#### Predicted changes in moment at the whisker base as the whisker rotates against an object

We now use *model 2* (Eq. 7) to compute the predicted changes in moment at the whisker base as the whisker is rotated against an object. Figure 6A plots the rate of change of moment at the base of the whisker as a function of contact distance for two different whisking velocities. To highlight the effects of taper (see APPENDIX B), results for the cylindrical whisker are also shown (gray traces). For both tapered and cylindrical whiskers, the steepest change of  $\dot{M}$  is for  $\frac{d}{L_{BT}} \leq 0.3$ , when the imposed force is closer to the vibrissal base. It is clear that  $\dot{M}$  goes to infinity for positions very close to the base. In addition,  $\dot{M}$  goes to zero at the tip of the tapered whisker, meaning that almost no moment is transmitted back to the base when contact is made very near the tip. Instead, the whisker tip might locally deflect and subsequently drag along the object. This suggests that the more distal regions of the whisker may be more sensitive to low-amplitude, high-frequency signals,

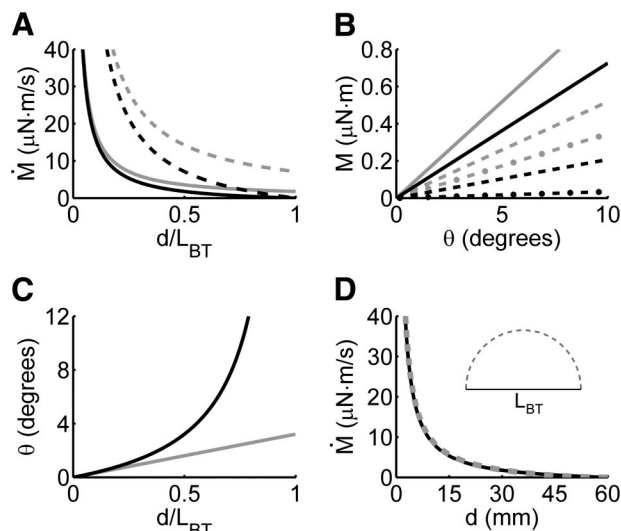


FIG. 6. *Model 2* provides relationships between rate of change of moment,  $\dot{M}$ , moment,  $M$ , deflection angle,  $\theta$ , and radial object distance,  $d$ . All simulations modeled whiskers with a Young's modulus of 3.5 GPa, a base radius of  $60 \mu\text{m}$  and a length of 6 cm. A: rate of change of moment vs. normalized contact distance for conical and cylindrical whiskers rotating at different velocities. Black curves represent relationship for a tapered whisker, whereas the gray curves are for a cylindrical whisker. Solid lines: velocity = 1 rad/s; Dashed lines: velocity = 4 rad/s. Rates of moment change for both whisker

shapes rapidly approach infinity for  $\frac{d}{L_{BT}} < \sim 0.3$ . B: moment as a function of whisker angle since contact with the object. Solid curves are for an object distance of  $0.3 L_{BT}$ , the dashed curves for an object distance of  $0.6 L_{BT}$ , and the dash-dotted curves for an object distance of  $0.9 L_{BT}$ . Black curve models a tapered whisker, and gray curves model a cylindrical whisker. C: whisker deflection as a function of normalized contact distance with an imposed  $0.1 \mu\text{N}\cdot\text{m}$  moment (whisker rotated against the object until  $0.1 \mu\text{N}\cdot\text{m}$  was reached). D: inherent whisker curvature has a negligible effect on rate of change of moment  $\dot{M}$ . This graph plots  $\dot{M}$  at the whisker base as the whisker is rotated against a point-object placed at different radial distances,  $d$ , out along the whisker. Solid black line indicates initial rate of moment change for a tapered, straight whisker (*model 2*). Dashed gray line indicates initial rate of moment change for a tapered whisker with an inherent curvature equal to that of a semi-circle (*inset*) found from numerical simulation. The two curves are virtually indistinguishable. Semi-circle inherent curvature is an extreme case and is much larger than that of any real rat whisker.

because these small signals can be amplified by resonance (Andermann et al. 2004).

Figure 6A also shows that the magnitude of  $\dot{M}$  is larger when the angular velocity  $\dot{\theta}$  is larger. This is an intuitive result, but the figure makes clear that the rat can obtain the same value of  $\dot{M}$  at the whisker base either by increasing whisking speed or by moving its snout closer to the object. This may suggest the existence of a “sweet spot” or “sweet combination” of object distance and whisking velocity. This location on the whisker would be constrained by the following criteria.

- If the snout is too close to the object, the moment may become so large that receptors in the follicle may saturate or the “motor” (i.e., the sling muscles) could max out and the whisker may barely even bend.
- If the snout is too far away from the object, the moment transmitted to the base may be below the rat's detection-threshold, or differences in moment may be difficult to resolve. Also, if contact occurs very close to the tip, the whisker will quickly fold in on itself and subsequently either flick past the object or drag along it.

- Different velocities will scale the curve in Fig. 6A. Faster velocities mean that better resolution will be obtained for objects further away.

Figure 6B plots the rate of moment change at the base of the whisker as a function of whisker angle,  $\theta$ . As mentioned earlier,  $\theta$  is the angle subtended since initial contact with the object and is interchangeable with time on the  $x$ -axis as long as  $\dot{\theta}$  is constant. Each curve in Fig. 6B represents a different object distance ( $0.3L_{BT}$ ,  $0.6L_{BT}$ , and  $0.9L_{BT}$ ). It is critical to understand that the linear relationship between  $\dot{M}$  and  $\theta$  does not mean that the whisker will bend linearly along its length. The proportionality constant between  $\dot{M}(x)$  and  $y(x)$  is different at each point  $x$  along the whisker. In addition, imposing a force at position  $2x$  does not make the whisker bend twice as much as if the force were imposed at position  $x$ . This can be seen in the uneven spacing of the lines for  $0.3L_{BT}$ ,  $0.6L_{BT}$ , and  $0.9L_{BT}$  in Fig. 6B.

#### Predicted changes in curvature at the whisker base as the whisker rotates into an object

It is clear from Eq. 1 that curvature and moment are directly proportional. The change in curvature at any point along a beam is equal to moment divided by the whisker bending stiffness,  $EI$ . Figure 6C plots the angular position of the whisker,  $\theta$ , as a function of normalized contact distance  $\frac{d}{L_{BT}}$ , for an imposed  $0.1\text{-}\mu\text{N}\cdot\text{m}$  moment. Simply put, this plot predicts how much the whisker will bend if the whisker is being actuated by a maximum moment of  $0.1\text{ }\mu\text{N}\cdot\text{m}$ . For a cylindrical beam, the relationship is purely linear. For a tapered beam, much less moment is required for the whisker to deflect past a distal object compared with a more proximal one.

#### Effects of inherent whisker curvature on moment sensed at the base

Finally, we now show that *model 2* holds for all realistic values of whisker curvature (and even much larger curvatures). A mechanical rule of thumb states that if the radius of curvature of a beam is  $\geq 10$  times its maximum cross-sectional depth, many fundamental principles of deformation analysis remain valid (Young and Budynas 2001). Geometrical analysis showed that the real rat whiskers used in this study exhibited a maximum curvature of 1.7 (units normalized to whisker arc length) along their length. A typical ratio of the radius of curvature to depth was  $\sim 250$ . The minimum ratio found along any whisker was  $\sim 100$ . Because the minimum value is much  $> 10$ , fundamental elasticity equations apply.

Numerical simulations were used to compare changes in  $\dot{M}$  profiles for a straight whisker and for a whisker with a large inherent curvature. To be conservative, we modeled the deformation of a whisker bent into the extreme shape of a semi-circle, which has a constant normalized curvature of  $\pi \approx 3.14$ . This is roughly twice the maximal curvature found for any of the real whiskers. Base-to-tip length for both models was 60 mm. Figure 6D shows the results of the simulation: the  $\dot{M}$  profiles for the straight and inherently curved whiskers overlap almost exactly. The inherent curvature has negligible effect on the moment that will be sensed at the whisker base.

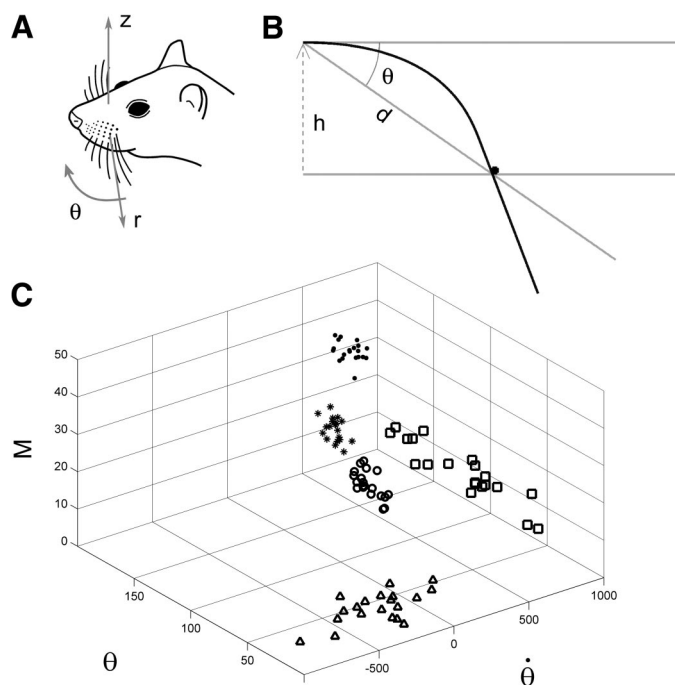


FIG. 7. Neural encoding of primary mechanical variables during translation and rotation. *A*: cylindrical coordinates are the most natural system in which to describe whisking movements of the rat. *B*: whisker deflection model presented in this paper can be used to describe deflections caused by translation and rotation. A straight, undeflected whisker is represented by the solid horizontal and slanted lines. The whisker either rotates  $\theta$  degrees or translates a distance  $h$ . Deflection by an object (black dot) at a radial distance,  $d$ , will eventually result in identical deflection profiles (black trace). *C*: proposed representation for 3 of the 4 mechanical variables found to be important in this study. Axes of the graph are angular position, angular velocity, and moment at the base of the whisker. Neural responses of Vg cells could be quantified by placing them within the state-space defined by these axes. In this schematic, each symbol represents spike of a ganglion neuron responsive to a particular combination of parameters. Magnitude of neural response is represented by number of data points (spike count), and variability in the response is represented by the 3-dimensional breadth of distribution. Triangles, for example, depict a cell sensitive to a particular combination of angular position (near  $40^\circ$ ) and velocity (between  $-800$  and  $250^\circ/\text{s}$ ), but not responsive to moment. Square symbols lie in the velocity-moment plane and represent a cell that responds roughly independent of position, but only to a particular combination of velocity and moment.

#### Effects of whisker or head translations compared with whisker rotations

As established by earlier studies (Szwed et al. 2003, 2006), and as schematized in Fig. 7A, cylindrical coordinates are the most natural system to describe whisking movements of the rat. Theta describes the rostral-caudal angle,  $z$  is the height of the whisker row, and  $r$  is the radial distance out along the whisker. This coordinate system is particularly suited to describe the rotational movements that most typically characterize whisking behavior.

Sometimes, however, rats' exploratory behaviors involve translational movements of the head instead of rotations of the whiskers. For example, a recent study showed that rats were able to discriminate the width of an aperture to within millimeter resolution using a translational "nose poke" through the aperture (Krupa et al. 2001). Rats were able to perform this task at above chance levels even when only one whisker remained on each side of the face. The authors did not propose an encoding mechanism for distance detection, but noted that

whiskers were “deflected rearward” as the rats entered the aperture.

Figure 7B shows that the models presented in this paper hold equally well for translation and rotation and can explain the results of the earlier study by Krupa et al. (2001). The models also apply to earlier studies that involve small-angle passive displacements of the whiskers in anesthetized rats (Leiser and Moxon 2006; Lichtenstein et al. 1990; Shoykhet et al. 2000; Webber and Stanley 2006). With knowledge of whisker length and base diameter, approximate Young’s modulus (3–4 GPa), the location of the imposed stimulus and its magnitude (which could take the form of a force, rotation or linear deflection), experimenters can now calculate approximately how much moment is experienced at the base of the whisker during passive displacement experiments. As will be shown in DISCUSSION, however, this may not be a very useful calculation to perform for passive displacement experiments.

The variables that this study has found to be important for shape extraction are angular position, angular velocity, moment (or equivalently, curvature), and rate of change of moment. This mechanical analysis suggests that a state-encoding scheme (Paulin 2004; Paulin and Hoffman 2001; Paulin et al. 2004) is a parsimonious and quantitatively rigorous way to represent the responses of Vg neurons. Figure 7C shows an example of a state-encoding scheme using three of the four mechanical variables. Neurons have a certain probability of firing a spike when the whisker is in a particular “state.” A state is uniquely defined by whisker position, velocity, moment, and moment-dot; in the example of Fig. 7C only three of the four variables are included. If necessary, velocity could be defined to have two dimensions (rostral-caudal and dorsal-ventral) to account for the directional sensitivity of the cells of velocity information (Jones et al. 2004). This would result in a higher dimensional space but would otherwise leave the state-encoding representation unchanged.

## DISCUSSION

### Technical considerations

**WHY DEVELOP AN ANALYTICAL MODEL?** This study has developed simple, analytical models for the deformation of rat vibrissae that account for vibrissal curvature as well as taper. The models are well matched by experimental results (Figs. 4 and 5). The advantage of an analytical model over the numerical method also presented in this paper is that it can be solved quickly and exactly, without use of a computer, to obtain a very close approximation to how a real whisker will bend. This is potentially useful to all investigators performing experiments in which the whiskers are deflected by an amount within the confines defined by Fig. 3C. Analytic models also make explicit the dependence of whisker bending properties on mechanical variables. Numerical simulations are required to precisely quantify bending of the whiskers in other cases. It is important to note that the change in curvature and the change in moment at every point along the whisker length are directly proportional, related through the whisker bending stiffness  $EI$ .

**YOUNG’S MODULUS AND WHISKER STIFFNESS.** Young’s modulus ( $E$ ) for biological materials is an approximation at best. This study found that  $E$  approximately equals 3–6 GPa, in line with previous estimates (3–4 GPa, Hartmann et al. 2003; 9 GPa,

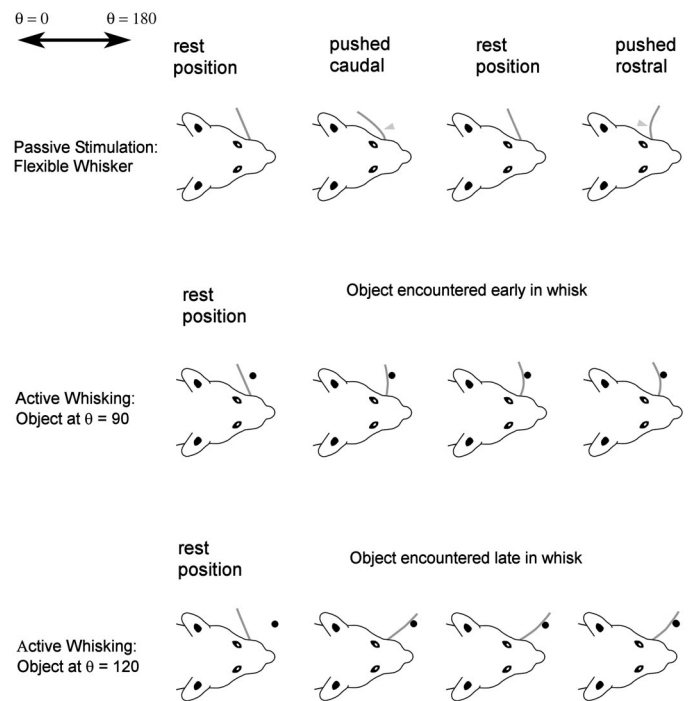


FIG. 8. Passive displacement experiments (top row) force a direct relationship between angular position and moment. In active whisking experiments (bottom 2 rows), moment changes at the base as the whisker deflects into an object placed at different angular positions.

Neimark et al. 2003; 3.5 GPa, Solomon and Hartmann 2006). A puzzling result of these experiments is that the value for  $E$  seemed to decrease as forces were imposed further from the whisker base (Fig. 5). There are at least four possible explanations for this result. First, the result could be taken at face value. The whisker material may vary with length in such a way as to result in lower  $E$  values further from the whisker base. Second, it is possible that the equivalent stiffness of the whisker decreases with whisker length. For example, if the whisker tapered parabolically instead of linearly, then the smaller cross sectional area as a function of length would result in an apparently lower  $E$  value. Third, Fig. 3C shows that the accuracy of the tapered-beam model decreases as the force is imposed further from the base. It is therefore possible that the decreased accuracy of *model 1* is directly responsible for the apparent change in Young’s modulus. This is consistent with the increase in error associated with the “best fit” Young’s modulus as deflections were imposed at increasing radial distances. Fourth, friction would have the largest effect on the most curved (shortest) whisker, thereby increasing the apparent value for  $E$ .

**IMPORTANCE OF MOMENT.** Almost all previous studies of the vibrissae have focused exclusively on kinematic variables, that is, angular position and its time derivatives. These variables are termed kinematic because they describe the motion of a body without consideration to the forces or moments that affect the motion. During active whisking, however, kinematic variables alone cannot provide a complete representation of all the information transmitted to the rat through its whiskers. Under active whisking conditions, the whisker could well be at the same angular position and yet experience very different moments at the base. Figure 8 shows some of the differences

between active and passive whisker displacements. The models presented in this study begin to consider the potentially important role that moment may play in conveying meaningful information to the rat.

For completeness, we note that both of these models would be considered “quasi-static,” because they assume that the movement of the whisker can be approximated so that at every point in time it is essentially at equilibrium. Assumptions for a quasi-static model require that all forces and moments are conservative and that the whisker has two physical constraints: the rigid connection at its base and at the contact point with the object. A fully dynamic (not quasi-static) treatment of the whisker would have to incorporate mass and inertial quantities and collision forces that may result in “whip.”

**RELATIVE IMPORTANCE OF WHISKER DIAMETER, LENGTH, CURVATURE, AND TAPER.** All equations in this study indicate that moment at the whisker base will depend on the base diameter of the whisker raised to the fourth power. Thus whisker diameter will have the largest influence of any single variable on the moment experienced at the whisker base. There is more tolerance for small deviations in whisker length. The inherent curvature of the whisker plays a relatively small role in determining how the deflected whisker will change shape, whereas in contrast, the taper of the whisker greatly affects how the whisker will bend and the moment transmitted to the base.

#### *Models are highly applicable to natural whisking behaviors*

Throughout the **METHODS** and **RESULTS**, we have been careful to emphasize the assumptions embedded in the models and the limitations that these assumptions impose. This careful exposition of modeling constraints may leave the impression that the models apply only under very limited conditions. It is therefore important to emphasize that our analysis is in fact very general and that versions of the models will hold even for very complex behaviors.

**MODELS CAN APPLY TO A WIDE RANGE OF BOUNDARY CONDITIONS: THE IMPORTANCE OF INSTANTANEOUS MEASUREMENT.** Moment at the whisker base will vary depending on how stiffly or loosely the whisker is held in the follicle, that is, on the boundary conditions in and near the follicle. The rat could presumably change follicular boundary conditions through muscular activation as well as by modulating blood flow to the follicular sinus (Scott 1955). The models in this study are based on clamped boundary conditions at the whisker base, but more realistic, tissue-like conditions might be modeled with a spring-mounted or a torsional-spring-mounted whisker. It is critical to note, however, that the fundamental results of this study will not change, even if boundary conditions are very different from the clamped condition modeled here. This is because the relationship between moment at the base and radial object distance will remain monotonic regardless of boundary conditions. As long as the rat can learn the monotonic function that relates these variables ( $M$  and  $d$ ), the method proposed here will work for radial distance extraction.

What happens if the rat changes the boundary conditions at the whisker base during the course of a whisk? *Equations 7 and 8* show that the rat can determine radial object distance based

on the instantaneous rate of change of moment. This means that the rat need only sense distance at a single instant during the whisk, and it does not matter if boundary conditions change before or after that instant. Recent behavioral data (Mitchinson et al. 2007) have shown that rats often use an exploratory strategy of “minimum impingement,” in which they tap, rather than sweep, their whiskers over objects. This suggests that the rat gains a sense of radial object distance in the first few milliseconds immediately after object contact. This strategy is consistent with the one determined to be most effective for radial distance extraction in a hardware model of the whiskers (Solomon and Hartmann 2006) and also helps avoid measurement complications caused by whisker slip along the object. Finally, we note that regardless of boundary conditions, the amount that the moment will change in a given time interval is directly related to the whisking velocity. We therefore suggest that variations in velocity over the trajectory of the whisk may be of particular behavioral importance to the rat during tasks that require estimates of object distance.

**MODELS CAN APPLY TO A WIDE RANGE OF ANGULAR DISPLACEMENTS, VELOCITIES, AND DISTANCES TO OBJECT CONTACT.** Numerous papers have shown that naturalistic rat behaviors use a large range of angular positions, velocities, and distances to object contact (Brecht et al. 1997; Carvell and Simons 1990, 1995; Guic-Robles et al. 1989; Polley et al. 2005; Vincent 1912). It might therefore be asked how the values for these variables presented here fit into these ranges. For example, over what range of angles, whisking amplitudes, and velocities, do the proposed models apply? The short answer is that the fundamental results of the models hold over virtually all distances to contact except very near the tip, all angular velocities, and all angular displacements. Figure 8 shows the broad applicability of the models and the differences between passive displacements and active whisking.

The rat-centered coordinate system for Fig. 8 is defined by  $\theta$  in the top left corner. A value of  $\theta = 0$  means that the whisker is completely retracted, pointed directly backwards toward the tail of the rat. A value of  $\theta = 180^\circ$  means that the whisker is completely protracted, pointed directly forward toward the snout of the rat. The *first row* of Fig. 8 shows passive deflection assuming that the whisker behaves as a flexible beam. In this case, pushing a point on the whisker backward or forward causes the whisker to bend and generates a moment at the whisker base. Consistent with the models presented in **RESULTS**, this figure assumes that the whisker is held rigidly at the base. Assume that the point on the whisker in contact with the stimulator is pushed to some value of  $\theta$ , different from the whisker’s rest position. The amount of whisker bending, and hence the moment generated at the base, depends directly on  $\theta - \theta_{\text{rest}}$ , that is, on the position to which the whisker is pushed. This means that there is no way to “decouple” the absolute angular position of the whisker (as measured at the point of stimulator contact) from the moment generated at the base.

The *second and third rows* of Fig. 8 show that active whisking permits decoupling of the values of absolute whisker position  $\theta$  and the moment generated at the base. In the second row, the whisker is actively protracted forward and behaves as a rigid body until it encounters the object at  $\theta \approx 90^\circ$ . As the whisker is increasingly protracted into the object, the whisker begins to bend, and the moment at the whisker base increases

with increased bending. In the third row, the whisker does not encounter an object until  $\theta \approx 120^\circ$ . Just as before, the whisker bends as it is protracted into the object, and the moment at the whisker base increases with increased bending. The only difference is that the bending is now occurring near  $\theta \approx 120^\circ$  instead of  $\theta \approx 90^\circ$ .

Examination of Fig. 8, rows 2 and 3, clearly shows that the models apply to the whisker encountering an object at any angular position. The models also apply regardless of the whisker's angular velocity. The rate of moment change at the whisker base depends directly on the angular velocity with which the whisker is protracted. By learning the relationship between moment change and angular velocity, the rat can extract radial object distance  $d$ . The *second* and *third rows* of Fig. 8 also show that the small angle approximation applies in all cases of initial object contact. When the whisker first makes contact with an object, the initial bending angle is zero. As the whisker presses by the object, the bending angle increases, and the angular deflection to which the model holds up depends on the object's radial distance, as depicted in Fig. 3C. As discussed above, we suggest that the rat gains a sense of radial object distance in the first few milliseconds immediately after object contact, exactly when the small angle approximation applies. Importantly, however, the fundamental result of this paper does not depend on small angles. Large bending angles will change the function that relates moment  $M$  and the radial distance  $d$ , but it will not change the fact that  $M$  and  $d$  are monotonically related for a given value of  $\theta$ . Thus as long as the rat can learn this relationship, a variation of the model will apply.

MODELS CAN BE ADAPTED TO APPLY TO MULTIPOINT CONTACT. The models, experiments, and analysis presented in this study have assumed frictionless point contact. This means that forces are assumed to be applied only normal to the vibrissa at the point of contact. However, recent studies from several laboratories have shown that rats engage objects and surfaces in complex ways, some of which have a large fraction of the whisker in contact with an object as it sweeps by (Carvell and Simons 1996). How do the models presented in this paper hold up under conditions of multipoint contact? The answer to this question has four components.

First, the initial contact of a whisker with an object will almost certainly be single-point, before the rest of the whisker has a chance to make contact with the object. As discussed above, we suggest that it is only the first few milliseconds after object contact that the rat needs to estimate object distance. Second, any force applied to the whisker can be divided into normal and tangential components. It seems likely that the rat is able to sense these components independently (Zucker and Welker 1969), which would permit not only extraction of radial distance, but also horizontal angle (Gopal and Hartmann 2007). Third, the principle of superposition states that any load distributed along a beam can be modeled as a resultant force  $F_R$  acting at a single point at the beam. This means that moment at the base can be calculated even for multipoint contact, provided that the appropriate location and magnitude  $F_R$  can be determined. Determining the magnitude and the location of the resultant force for multipoint contact during natural behaviors will be an interesting future adaptation to the model. Finally,

point-contact is standard in passive-stimulation experiments in the anesthetized animal.

### *Behavioral implications and relevance*

WHY DO RATS NEED TO EXTRACT RADIAL DISTANCE WITH A SINGLE WHISKER AT ALL? It could be argued that during natural exploratory behavior the rat has use of multiple vibrissae, and thus might not need to figure out radial distance along each whisker. Instead, the rat could compare contact between whiskers. We can imagine two ways that this comparison could occur: 1) the rat could either have a sense for the relative lengths of each of its whiskers and compare contact between them or 2) the rat could "mold" its entire whisker array around an object and determine object features by the relative moments felt at the base of each whisker. The rat could also combine the two methods.

Let us suppose that the rat has a sense for, or "knows" the relative length of each of its whiskers. If a whisker of length  $L$  touched an object, but a whisker of length  $L - \Delta L$  did not, the rat could infer that the object was located at a distance between those two values, after accounting for different whisker base locations. There are at least three problems with this technique. First, a recent paper has shown that rats have tactile "hyper-acuity;" they can distinguish between differences less than  $\Delta L$  (Knutsen et al. 2006). Second, it has been shown that rats can make accurate distance judgments with a single whisker remaining on each side of the face (Krupa et al. 2001). Third, during complex natural behaviors whiskers are very likely to contact objects anywhere along their length, not just at their tips. How can the rat know where this contact has taken place, given that there are no receptors on the whisker itself? This study provides a good explanation for how the rat could obtain this information.

Now let us suppose that the rat shapes or "molds" its whisker array around an object. What would it mean, mechanically, for this to occur? It would mean that the whiskers are pushed against the object until the rat is able to sense that the whiskers have touched the object. The only possible mechanical cues that could provide this information are moment and force. No other variable can describe the "push" on the receptors in the follicle. As the whiskers are molded around the object, the rat must determine where along each whisker's length it has touched the object. This is one key point of this study.

BEHAVIORAL CONSEQUENCES OF CURVATURE AND TAPER. An intriguing result of this study is that the inherent curvature of the whisker plays a relatively small role in determining deflected whisker shape for a given force and force location (Fig. 3C). Furthermore, the initial rate of change of moment sensed at the base is not affected by inherent whisker curvature, regardless of where along its length the whisker hits an object. This suggests that the curvature of the whisker may serve some other behavioral function, such as maximizing the sensory volume searched during whisking. In contrast, the taper of the whisker plays a substantial role in determining the way the whisker will bend and the moment that will ultimately be transmitted to the whisker base (see APPENDIX B). For a particular force imposed at a given distance out along the whisker, the tapered whisker will bend substantially further, yet transmit the same moment to the base as a cylindrical whisker of the

same base diameter. The biomechanics thus ensure that large deflection amplitudes of the distal parts of the whisker are required to transmit a moment to the base. This makes sense behaviorally, because the most distal parts of the whiskers are often deflected through very large amplitudes as they brush past an object.

**COMPLEMENTARITY OF VIBRATIONS AND BENDING.** Does whisker taper make the whisker “more sensitive” or “less sensitive” near the tip? The answer depends on the definition of “sensitive.” The taper makes the whisker bend more for the same imposed force (more sensitive), but it reduces the moment ultimately transmitted to the base (less sensitive). This suggests that object contact near the tip will tend to cause the whisker to abruptly bend in on itself (or otherwise flick past), and therefore implies that the tip would be useful if vibrations were amplified during resonance (Andermann et al. 2004; Hartmann et al. 2003; Neimark et al. 2003). This in turn suggests that differential extraction of texture and shape may occur at different locations along the whisker as well as within two different frequency regimens. The two types of information could be simultaneously extracted in the same whisking motion: vibrations can be superimposed on the overall deflection of the whisker.

**DO RATS “TAP” OR “SWEEP” THEIR WHISKERS?** This study showed that radial object distance can be determined by examining how moment at the whisker base changes with angular position  $\theta$  as the whisker is increasingly deflected into an object. Although outside the scope of this study, it is also possible to show that local object curvature can be determined by looking at the second derivative of moment with respect to time as the whisker is increasingly deflected into an object. If rats “tap” their whiskers against an object, they would be able to build up a representation of the object point by point. If rats “sweep” their whiskers against an object, they would be able to make use of local curvature information in determining object shape as well as texture. Combining these two strategies might help maximize the sensory information acquired. Behavioral studies to investigate these two potential exploratory strategies are currently underway. Data from Mitchinson et al. (2007) suggest that tapping tends to be the preferred strategy.

#### *Physiological correlates and implications for higher-order neural processing*

**RESPONSES OF TRIGEMINAL GANGLION NEURONS.** In a recent study, Szwed et al. (2006) recorded from Vg neurons while stimulating the facial motor nerve to rotate whiskers into objects placed at varying radial distances. Their results showed that a subset of Vg neurons (called “touch” cells) encode radial distance primarily by increases in firing rate. This study offers a clear biomechanical explanation for these recent physiological results.

For example, Fig. 2, C and D, in Szwed et al. (2006), shows that touch cells increase their firing rate as the object is placed closer to the whisker base. This is exactly what would be expected from Fig. 6A of this study, if the Vg neurons were responding to rate of change of moment (Szwed et al., Fig. 2C) and to moment (Szwed et al., Fig. 2D). Figure 4 of Szwed et al. shows that higher velocities at the instant of object contact also increase the firing rate of Vg neurons. This result is also

predicted by the data in Fig. 6A of our study. Faster velocities scale the relationship between moment and radial object distance (compare solid and dashed lines). This makes good intuitive sense, because the rate of change of moment will be larger if the whisker is pushed faster past the object. Thus this study strongly suggests that the touch-sensitive Vg neurons found by Szwed et al. are responding to the moment and rate of change of moment at the whisker base.

**STATE ENCODING.** Responses of Vg neurons have been classified according to two schemes. The first method divides Vg neurons into rapidly adapting (RA) and slowly adapting (SA) cells (Leiser and Moxon 2006; Lichtenstein et al. 1990; Shoykhet et al. 2000). It has recently been shown that the RA and SA properties of Vg cells are modulated by the direction of movement (Jones et al. 2004). The second method classifies Vg responses by their activity during active touch. Neurons are described as “whisking,” “touch,” and “whisking-touch” cells (Szwed et al. 2003, 2006).

This study has shown that whisker angular position, angular velocity, moment, and the time derivative of moment provide enough information to describe the 3D coordinates of an object, as well as static deflection information. This mechanical representation most naturally lends itself to a state-encoding scheme in which these variables form the axes of a state-space. The activity of a neuron can be represented by placing a data point at the correct place in the state space every time that neuron fires. The responses of RA and SA cells, as well as whisking, touch, and whisking-touch cells would form trajectories through the space. In no way do we intend to suggest that Vg neurons cleanly encode any mechanical parameters or that the Vg is in any way “imposing” state-encoding on the incoming data. Vg neurons merely respond to highly nonlinear signals from mechanoreceptors in the follicle. The state-encoding scheme shown in Fig. 7C is intended as a conceptual tool for grappling with the real-world complexity of Vg neuron responses.

We suggest that the scheme proposed in Fig. 7C will be particularly useful for precisely quantifying the spatiotemporal patterns of activity across the whisker array resulting from different behaviors. State encoding inherently permits a spectrum of response types and allows us to examine how the Vg neurons “cover” the relevant behavioral space of the rat. This may ultimately allow us to make strong predictions for coding strategies in the trigeminal nuclei.

**COMPUTATIONS OF GRADIENTS OF DISTANCE AND CURVATURE AT HIGHER STAGES OF THE NERVOUS SYSTEM.** It is well known that the rat often combines whisking behavior with small, periodic head movements that tend to be temporally synchronized with whisking (Brecht et al. 1997; Hartmann et al. 2000; Welker 1964). These head movements seem to allow the rat to obtain multiple, overlapping samples of the object. If, as we suggest, information about moment is encoded in trigeminal ganglion responses, how might it be subsequently processed in the trigeminal nuclei? We propose that during object exploration, the trigeminal nuclei are used to compute gradients of object distance and gradients of object curvature, as follows. 1) Within a single whisk, ganglion neurons provide information about the radial distance at which each whisker has contacted an object. The trigeminal nuclei could then compute the local curvature of the object by calculating gradients of these dis-

tances. 2) Across whisks, head movements permit the rat to compare overlapping whisked samples of the object. The trigeminal nuclei could compute gradients of local object curvatures to reconstruct the entire object shape. A very similar strategy may be used by humans as they perform exploratory hand movements that enclose objects and follow object contours (Lederman and Klatzky 1987).

WHAT TYPE OF LEARNING IS REQUIRED OF THE RAT WERE IT TO CALCULATE RADIAL DISTANCE ACCORDING TO THE MODEL PROPOSED HERE? Equation 8 relates moment at the whisker base to object distance through the parameters  $C$  and  $L_{BT}$ . This in turn suggests that the rat would need some “knowledge” of these parameters, which implicitly include parameters such as Young’s modulus and whisker radius. We do not suggest, however, that the rat “knows”  $C$  or  $L_{BT}$  as numbers. Instead, we suggest that, through interactions with the environment, the rat gains implicit knowledge of the mechanical properties of its body. The most general result of this study is that the rate of change of moment at the base is a curve that monotonically decreases with object radial distance, and this curve scales linearly with whisking velocity. This means that object distance  $d$  can always be uniquely inferred from measurement of  $M$  for any given whisking velocity  $\theta$ . The rat must learn the shape of the function that relates  $M$ ,  $d$ , and  $\theta$  through interaction with the environment. As the whiskers get damaged, fall out, grow back, age, we expect that it will feel “odd” to the rat at first, just as when you put on gloves, the movements of your hands feel different. You have to “learn” the curves that relate a commanded exploratory movement to a particular sensory input. This is all that our models require of the rat.

#### “Take home” messages for investigators of the vibrissal system

This paper is by necessity replete with technical details. We want to ensure that the following points are clear.

1) Change in curvature of the whisker and moment (caused by whisker deflection) are always proportional. They are related through the quantity  $EI$ , representing the whisker bending stiffness. Both curvature and moment vary as a function of arc length for a deflected whisker, up until the point of contact. A whisker cannot be said to have a single curvature, and it cannot be said to have a single moment. One can only talk about curvature at a point on the whisker and moment at a point on the whisker. A useful point to talk about is often the whisker base, where the rat would actually sense these variables.

2) If an experimenter is performing passive displacement experiments, in which a whisker is grabbed and shaken, it will not be particularly useful to calculate the moment at the base of the whisker. In passive experiments, the moment at the whisker base is linearly related to angular position of the whisker. (Fig. 8, row 1; Eq. 6). This is very different from situations that can arise during active whisking (Fig. 8, rows 2 and 3).

3) If an experimenter performing passive displacement experiments for some reason did wish to compute the moment at the whisker base, it can be calculated from Eq. 6. The experimenter would need to measure the base-to-tip length and base diameter of the whisker, the angular position of the whisker, and the radial distance from the whisker base to the contact location. Both models 1 and 2 will apply to almost all passive

deflection experiments to date, but limitations on their use are shown in Fig. 3C.

4) Kinematic descriptions of whisker trajectories are not sufficient to describe the information available to the rat during active behaviors. During active whisking, the whisker can experience very different moments while its base is at the same angular position (Fig. 8, rows 2 and 3). A complete description of the information available to the rat during active behaviors must include moment, or its geometrical analog, curvature. To ensure the use of our equations to experimentalists, we have expressed them both in terms of moment and curvature. If one knows the curvature at the whisker base (say from high-speed video), one can estimate the moment at the base. Conversely, if one knows the moment at a point along the whisker (say from contact with a load cell), one can estimate the curvature near the whisker base.

5) The inherent curvature of the whisker negligibly affects the dependence of the rate of change of moment on radial distance. In contrast, the whisker taper has a large influence on this property.

6) Vibrations of the whisker generated by object contact near the tip are a natural complement to the low-frequency moments that can be generated anywhere along the whisker length. This is likely to permit the simultaneous extraction of texture and shape.

7) The rat could extract radial object distance by keeping track of the rate of change of moment at the whisker base along with whisker angular velocity. This proposed computation for radial distance works for both translation and rotation and works even if the rat only keeps track of instantaneous rates of change in these variables. In theory, this allows the computation to be performed at every instant in time.

8) The mechanism for computing radial distance proposed in this study can account for many of the recently discovered physiological response properties of Vg neurons during active touch (Szwed et al. 2006).

9) The mechanical description of whisking variables presented here has shown that angular position, angular velocity, moment, and the time derivative of moment, can completely describe the dynamic-state of the whisker. This result naturally lends itself to a state encoding scheme, describing the dynamic states of an oscillating cantilever beam. This representation is likely to be particularly useful when quantifying responses of Vg neurons during active behaviors, and responses at subsequent stages of processing (e.g., the trigeminal nuclei).

10) We propose that the shape of an object can be reconstructed by finding gradients of distance ( $r$ ,  $\theta$ ,  $z$ ) over the sensor array and gradients of curvature across different positions of the entire array.

#### APPENDIX A

##### ANALYTIC SOLUTION OF THE SMALL-ANGLE DEFLECTION OF A TAPERED (CONICAL) CANTILEVER BEAM

Elasticity equations (Euler 1744; Love 1944; Timoshenko and Goodier 1970) relate the curvature  $\kappa$  of a cantilever beam to the moment  $M$  at its base

$$\kappa = \frac{d^2y}{dx^2} = \frac{M}{EI} \quad (A1)$$

where

$$M = \begin{cases} F(a-x) & 0 \leq x \leq a \\ 0 & a \leq x \leq L \end{cases}$$

In (1),  $F$  is the force exerted at a distance  $a$  from the base of the beam,  $y(x)$  is the vertical displacement of the beam at each  $x$  (horizontal) location,  $E$  is Young's modulus (also called the elastic modulus) and  $I$  is the second areal moment of inertia. For a cylinder

$$I = \frac{\pi r^4}{4} \quad (\text{A2})$$

For a cone, however,  $r$  varies with length as

$$r = r_{\text{base}} \left(1 - \frac{x}{L}\right) \quad (\text{A3})$$

Substituting Eq. A3 into Eq. A2 yields

$$I = \alpha(L-x)^4,$$

where  $\alpha$  is a constant defined as

$$\alpha = \left(\frac{\pi}{4}\right) \left(\frac{r_{\text{base}}}{L}\right)^4 \quad (\text{A4})$$

Inserting expressions for  $I$  and  $M$  into Eq. A1 for  $x \leq a$  gives

$$\frac{d^2y}{dx^2} = \left(\frac{F}{E\alpha}\right)(a-x)(L-x)^{-4} \quad (\text{A5})$$

Integrating once with respect to  $x$  yields

$$\frac{dy}{dx} = \left(\frac{F}{E\alpha}\right) \left[ \frac{1}{2(L-x)^2} - \frac{(L-a)}{3(L-x)^3} \right] + C_1 \quad (\text{A6})$$

And integrating again with respect to  $x$  yields

$$y(x) = \left(\frac{F}{E\alpha}\right) \left[ \frac{(a-L)}{6(L-x)^2} + \frac{1}{2(L-x)} \right] + C_1x + C_2 \quad (\text{A7})$$

To find the constant of integration  $C_1$  we note that  $\frac{dy}{dx}$  at  $x = 0$  must equal zero, so that Eq. A6 becomes:

$$0 = \left(\frac{F}{E\alpha}\right) \left[ \frac{1}{2(L-x)^2} - \frac{(L-a)}{3(L-x)^3} \right] + C_1 \quad (\text{A8})$$

Solving for  $C_1$  gives

$$C_1 = \left[ \frac{-F(L+2a)}{6E\alpha L^3} \right] \quad (\text{A9})$$

To find the constant of integration  $C_2$ , we note that  $y$  at  $x = 0$  must equal zero, so that Eq. A7 becomes

$$0 = \left(\frac{F}{E\alpha}\right) \left[ \frac{(a-L)}{6(L-x)^2} + \frac{1}{2(L-x)} \right] + 0 + C_2 \quad (\text{A10})$$

Solving for  $C_2$  gives

$$C_2 = \left( \frac{-F(2L+a)}{6E\alpha L^2} \right) \quad (\text{A11})$$

Substituting our expressions for  $C_1$ ,  $C_2$ , and  $\alpha$  back into Eq. A7 we find

$$y(x) = \frac{2FL^4}{3E\pi r_{\text{base}}^4} \left[ \frac{(a-L)}{(L-x)^2} + \frac{3}{(L-x)} - \frac{(L+2a)x}{L^3} - \frac{(a+2L)}{L^2} \right], \quad x \leq a \quad (\text{A12})$$

which simplifies to the top half of Eq. 4

To solve for the deflection at values of  $x$  greater than or equal to  $a$ , we note that the moment is zero. This means we can write

$$y(x) = y(a) + \left. \frac{dy}{dx} \right|_{x=a} (x-a) \quad (\text{A13})$$

Substituting in Eq. A6 evaluated at  $x = a$  gives

$$y(x) = \frac{2FLa^2}{3E\pi r_{\text{base}}^4} \left[ \frac{3Lx - La + 2ax}{(L-a)^2} \right], \quad x \geq a \quad (\text{A14})$$

## APPENDIX B

### EFFECTS OF TAPER ON WHISKER DEFORMATION

We used *model 1* as expressed in Eq. 4 of the main text, to explore two important consequences of the tapered geometry on whisker deformation, as would occur when a real whisker contacted an object. First, whisker taper ensures that the ratio between the displacement at some distance,  $a$ , and the force applied at  $a$  increases faster with  $a$  for the tapered whisker than for the cylindrical whisker. Intuitively, this makes sense: as a given force is exerted at increasing distances from the base, a tapered whisker will bend more than a cylindrical whisker. Figure A1 shows this effect for a 50- $\mu\text{N}$  force exerted at 10, 20, and 30 mm along the length of a 60-mm whisker with a base radius of 100  $\mu\text{m}$ . For the force applied closest to the whisker base ( $a = 10$  mm), the equations describing cylindrical and tapered whiskers yield almost the same deflected whisker shape. As the value of  $a$  increases, however, the two results diverge, with the tapered whisker deflecting far more than its cylindrical counterpart.

Figure A1B shows displacement-force curves for models of cylindrical and tapered whiskers for forces applied at the same values distance  $a$  as in Fig. A1A. In Fig. A1B, each value on the  $y$ -axis indicates the vertical deflection at point  $a$  along the whisker for the corresponding force  $F$  on the  $x$ -axis. In other words, Fig. A1B indicates how much a given whisker will deflect when a force is applied at point  $a$ , for both the tapered and cylindrical beams. In both cases, the force  $F$  increases linearly with the deflection  $y(a)$  (as can be seen directly in Eq. 4), but the displacement associated with a given force is considerably larger for the tapered whisker than for the cylindrical whisker.

The above analysis has indicated that (for a given force imposed at a given distance) a cylindrical whisker will deflect less than a tapered whisker of the same base radius. This result is not surprising because the radius (and hence the stiffness) of the tapered whisker at every point between the base and the contact point is smaller than the radius of the cylindrical whisker. We next asked: what happens when we apply the same force to cylindrical and tapered whiskers, but choose the radius of the cylindrical whisker to match the radius of the tapered whisker at the point where the force is imposed? The answer is shown in Fig. A1, C and D. The cylindrical whisker now deflects more than the tapered whisker. Again, this result should be somewhat intuitive, because of the difference in radius profiles from whisker base to contact-point.

Thus one consequence of whisker taper is to ensure a steeper relationship between displacement and force closer to the tip of the whisker. This result is summarized in Fig. A1E, which plots the deflection  $y(a)$  as a function of  $a$ , for a 50- $\mu\text{N}$  force imposed at  $a$ . The curve for the tapered whisker (base radius 100  $\mu\text{m}$ ) falls between the curves for cylindrical whiskers of base radii 50 and 100  $\mu\text{m}$ . The effect is easier to observe in Fig. A1F, which plots the identical data as Fig. A1E, but on a log-log scale. Here it can be seen that the deflection of the tapered whisker initially matches the deflection of the cylindrical whisker with the larger radius, but as  $a$  increases the trace curves upward toward the curve representing deflections of the smaller cylindrical whisker. The tapered geometry thus specifically

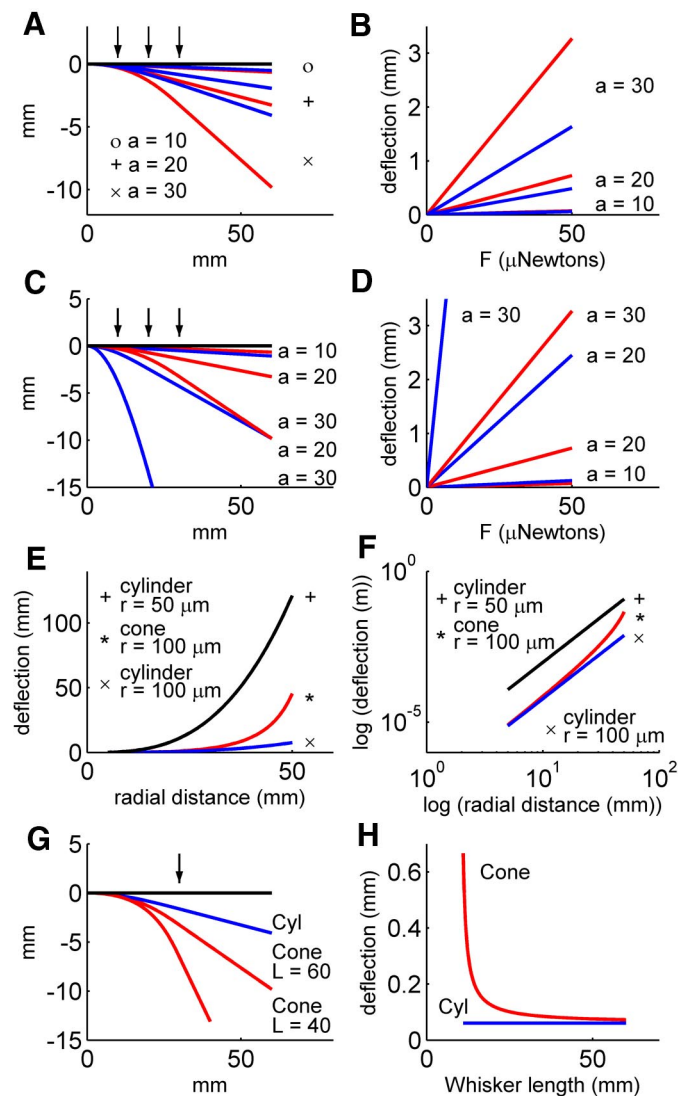


FIG. A1. Cylindrical (blue) vs. tapered (red) beam models. For all graphs, Young's modulus was assumed to be 3.5 GPa. **A:** deformations of ideal cylindrical and tapered cantilever beams under a vertical force  $F$  imposed a distance  $a$  from the base, for three different horizontal values of  $a$ . Both whiskers have a length  $L = 60$  mm and a base radius  $r_{\text{base}} = 100 \mu\text{m}$ . **B:** theoretical force-displacement curves for cylindrical and tapered beams for the same values of horizontal distance  $a$  as in part A. **C:** deflections resulting from an imposed vertical force,  $F$ , in the case that the tapered and cylindrical beams have matching radii at  $a$ , for  $a = 10, 20,$  and  $30$  mm. Arrows represent the locations of the imposed forces. **D:** force-deflection curves for cylindrical and tapered beams with matching radii at  $a$ , for  $a = 10, 20,$  and  $30$  mm. **E:** deflection of two cylindrical beams (base radii of  $50$  and  $100 \mu\text{m}$ ) and one conical beam (base radius of  $100 \mu\text{m}$ ) for a  $50 \mu\text{N}$  force, showing the effect of whisker taper. **F:** deflections of the same cases as **E** on a log-log scale. **G:** when a force is imposed  $30$  mm from the base, the length of the whisker does not affect how a cylindrical whisker will bend: the single blue trace shows results for both a  $60$  mm and a  $40$  mm whisker. In contrast, the shorter ( $40$  mm) conical whisker bends much more than the longer ( $60$  mm) whisker (red traces), when the same force is applied at the same position. **H:** relationship between deflection and whisker length, for a force applied at  $10$  mm. Deflections of the cylindrical whisker are unaffected by total whisker length (blue trace is a constant value). In contrast, deflections of the conical whisker fall off sharply with whisker length (red trace).

accentuates the magnitude of deflection that will occur further out along the length of the whisker.

A second difference between the equations for tapered and cylindrical whiskers is that deflections in the tapered case depend strongly

on the whisker length,  $L$ , whereas the deflections of the cylindrical case are indifferent of whisker length. In other words, how a whisker will react to a given imposed force depends on its total length. This effect is shown in Fig. A1G, which compares the deflections of cylindrical and tapered whiskers of two different lengths ( $40$  and  $60$  mm), but with the same base radius ( $100 \mu\text{m}$ ). In all cases the same magnitude force is applied  $30$  mm from the base. The cylindrical whisker bends the same amount regardless of length, and so only one curve is seen (blue line). In contrast, the short tapered whisker bends considerably more than the longer tapered one (red lines).

The effect of whisker length is further characterized in Fig. A1H. We simulated a  $50\text{-}\mu\text{N}$  force acting  $10$  mm from the base of a whisker whose length varied from  $11$  to  $60$  mm, but whose radius was held constant. The vertical deflection at the location of the imposed force ( $10$  mm from the base) was plotted as a function of whisker length for both cylindrical and tapered whiskers. As described for Fig. A1G, the deflection of a cylindrical whisker does not vary with overall whisker length, and so there is only one curve (blue line). In contrast, shorter tapered whiskers deflect far more than longer ones (red lines). As whisker length increases, the tapered result asymptotes to the cylindrical result. The implication for real rat whiskers is that for a force imposed at a particular distance (say  $10$  mm), longer whiskers will deflect much less than shorter ones. This result would hold true even if the base radii of all whiskers were the same. This result would not hold true if the whiskers were cylindrical.

#### ACKNOWLEDGMENTS

We thank Drs. Christopher Assad, Cate Brinson, Mike Coleman, and Mike Paulin for useful discussions.

#### GRANTS

We gratefully acknowledge the support of the Telluride Workshop on Neuromorphic Engineering, which brought three of the authors into collaboration. As part of the workshop, seed funding for early portions of this research was provided by NSF Research Coordination Network Grant IBN0129928, Avis Cohen P.I. Middle portions of the work were sponsored by the Bio-Inspired Technologies and Systems/CISM at NASA's Jet Propulsion Laboratory, and the later portions of the work were funded by NSF award IOB0446391 to M. J. Hartmann.

#### REFERENCES

- Ahissar E, Arieli A. Figuring space by time. *Neuron* 32: 185–201, 2001.
- Ahissar E, Sosnik R, Haidarliu S. Transformation from temporal to rate coding in a somatosensory thalamocortical pathway. *Nature* 406: 302–306, 2000.
- Andermann ML, Ritt J, Neimark MA, Moore CI. Neural correlates of vibrissa resonance: band-pass and somatotopic representation of high-frequency stimuli. *Neuron* 42: 451–463, 2004.
- Brecht M, Preilowski B, Merzenich M. Functional architecture of the mystacial vibrissae. *Behav Brain Res* 84: 81–97, 1997.
- Carvell GE, Simons DJ. Biometric analyses of vibrissal tactile discrimination in the rat. *J Neurosci* 10: 2638–2648, 1990.
- Carvell GE, Simons DJ. Task-related and subject-related differences in sensorimotor behavior during active touch. *Somat Mot Res* 12: 1–9, 1995.
- Ebara S, Kumamoto K, Matsuura T, Mazurkiewicz JE, Rice FL. Similarities and differences in the innervation of mystacial vibrissal follicle-sinus complexes in the rat and cat: a confocal microscopic study. *J Comp Neurol* 449: 103–119, 2002.
- Euler, L. *Eneström Number 65: Methodus Inveniendi Lineas Curvas Maximi Minime Proprietate Gaudentes, Sive Solutio Problematis Isoperimetricali Latissimo Sensu Accepti*. Geneva, Switzerland: Marcum-Michaellem Bousquet and Socios, 1744.
- Gopal V, Hartmann MJZ. Using hardware models to quantify sensory data acquisition across the rat vibrissal array. *J Bioinspiration Biomimetics* In press.
- Guic-Robles E, Valdivieso C, Guajardo G. Rats can learn a roughness discrimination using only their vibrissal system. *Behav Brain Res* 31: 285–289, 1989.
- Hartmann MJ. Active sensing capabilities of the rat whisker system. *Autonomous Robots* 11: 249–254, 2000.

- Hartmann MJ, Johnson NJ, Towal RB, Assad C.** Mechanical characteristics of rat vibrissae: resonant frequencies and damping in isolated whiskers and in the awake behaving animal. *J Neurosci* 23: 6510–6519, 2003.
- Jones LM, Lee S, Trageser JC, Simons DJ, Keller A.** Precise temporal responses in whisker trigeminal neurons. *J Neurophysiol* 92: 665–668, 2004.
- Knutsen PM, Pietr M, Ahissar E.** Haptic object localization in the vibrissal system: behavior and performance. *J Neurosci* 26: 8451–8464, 2006.
- Krupa D, Matell M, Brisben A, Oliveira L, Nicolelis MAL.** Behavioral properties of the trigeminal somatosensory system in rats performing whisker-dependent tactile discriminations. *J Neurosci* 21: 5752–5763, 2001.
- Lederman SJ, Klatzky RL.** Hand movements: a window into haptic object recognition. *Cogn Psychol* 19: 342–368, 1987.
- Leiser S, Moxon K.** Relationship between physiological response type (RA and SA) and vibrissal receptive field of neurons within the rat trigeminal ganglion. *J Neurophysiol* 95: 3129–3145, 2006.
- Lichtenstein SH, Carvell GE, Simons DJ.** Responses of rat trigeminal ganglion neurons to movements of vibrissae in different directions. *Somat Mot Res* 7: 47–65, 1990.
- Love AEH.** *A Treatise on the Mathematical Theory of Elasticity*. New York: Dover, 1944.
- Mitchinson B, Martin CJ, Grant RA, Prescott TJ.** Feedback control in active sensing: rat exploratory whisking is modulated by environmental contact. *Proc Royal Soc B* 274: 1035–1041, 2007.
- Mosconi TM, Rice FL, Song MJ.** Sensory innervation in the inner conical body of the vibrissal rollicle-sinus complex of the rat. *J Comp Neurol* 328: 232–251, 1992.
- Neimark MA, Andermann ML, Hopfield JJ, Moore CI.** Vibrissa resonance as a transduction mechanism for tactile encoding. *J Neurosci* 23: 6499–6509, 2003.
- Paulin MG.** System identification of spiking sensory neurons using realistically constrained nonlinear time series models. In: *Advances in Processing and Pattern Analysis of Biological Signals*, edited by Gath I, Inbar G. New York: Plenum, 2004.
- Paulin MG, Hoffman L.** State-space receptive fields of semicircular canal afferent neurons in the bullfrog. *Neurocomputing* 38-40: 293–298, 2001.
- Paulin MG, Hoffman L, Assad C.** Dynamics and the single spike. *Neural Networks* 15: 987–994, 2004.
- Polley DB, Rickert J, Frostig RD.** Whisker-based discrimination of object orientation determined with a rapid training paradigm. *Neurobiol Learn Mem* 83: 134–142, 2005.
- Rice FL, Fundin BT, Arvidsson J, Aldskogius H, Johansson O.** Comprehensive immunofluorescence and lectin binding analysis of vibrissal follicle sinus complex innervation in the mystacial pad of the rat. *J Comp Neurol* 385: 149–184, 1997.
- Scott M.** Blood supply of mystacial vibrissae. *Nature* 175: 395–396, 1955.
- Shoykhet M, Doherty D, Simons DJ.** Coding of deflection velocity and amplitude by whisker primary afferent neurons: implications for higher level processing. *Somat Mot Res* 17: 171–180, 2000.
- Solomon JH, Hartmann MJ.** Robotic whiskers used to sense features. *Nature* 443: 525, 2006.
- Szwed M, Bagdasarian K, Ahissar E.** Encoding of vibrissal active touch. *Neuron* 40: 621–630, 2003.
- Szwed M, Bagdasarian K, Blumenfeld B, Barak O, Derdikman D, Ahissar E.** Responses of trigeminal ganglion neurons to the radial distance of contact during active vibrissal touch. *J Neurophysiol* 95: 791–802, 2006.
- Timoshenko S.** *Theory of Elasticity*. New York: McGraw-Hill, 1970.
- Vincent SB.** The function of the vibrissae in the behavior of the white rat. *Behav Monogr* 1: 7–85, 1912.
- Webber R, Stanley G.** Transient and steady-state dynamics of cortical adaptation. *J Neurophysiol* 95: 2923–2932, 2006.
- Welker WI.** Analysis of sniffing of the albino rat. *Behaviour* 22: 223–244, 1964.
- Young W, Budynas R.** *Roark's Formulas for Stress and Strain*, New York: McGraw-Hill Professional, 2001.
- Zucker E, Welker WI.** Coding of somatic sensory input by vibrissae neurons in the rat's trigeminal ganglion. *Brain Res* 12: 138–156, 1969.